UNILE-CBR-2001-3
OUTP-01-33P

Susy QCD and High Energy Cosmic Rays 1.

Fragmentation functions of Susy QCD

Claudio Corianò[1] and Alon E. Faraggi[2]

[1] *Dipartimento di Fisica*
Universita' di Lecce
I.N.F.N. Sezione di Lecce
Via Arnesano, 73100 Lecce, Italy

[2] *Theoretical Physics Department*
University of Oxford, Oxford, OX1 3NP, United Kingdom

Abstract

The supersymmetric evolution of the fragmentation functions (or timelike evolution) within $N = 1$ QCD is discussed and predictions for the fragmentation functions of the theory (into final protons) are given. We use a backward running of the supersymmetric DGLAP equations, using a method developed in previous works. We start from the usual QCD parameterizations at low energy and run the DGLAP back, up to an intermediate scale -assumed to be supersymmetric- where we switch-on supersymmetry. From there on we assume the applicability of an $N = 1$ supersymmetric evolution (ESAP). We elaborate on possible application of these results to High Energy Cosmic Rays near the GZK cutoff.

[1] E-mail address: Claudio.Coriano@le.infn.it
[2] faraggi@thphys.ox.ac.uk

1 Introduction

The Standard Model of elementary particle physics successfully accounts for all the observed particle properties. Its remarkable success suggests the possibility that it correctly describes the particle properties up to energy scales which far exceed the currently accessible energy scales. Indeed, this possibility has been entertained in the explorations of Grand Unified, and Superstring, Theories. Additionally, the spectacular confirmation of the Standard Model in high energy colliders, as well as the proton longevity and suppression of left–handed neutrino masses, provide strong support for the grand desert scenario and unification. The question then is how are we going to find out whether this is indeed the path chosen by nature, as direct signatures at LHC/NLC will be able to probe the desert only up to a few TeV. Therefore we need new tools to achieve this. An example of such a probe that has been used with great success is that of the gauge coupling unification. The general methodology in this respect is to extract the gauge couplings from experiments that are performed at the accessible energy scales. Based on concrete assumptions in regard to the particle content in the desert, the couplings are then extrapolated to the high energy scale and the unification hypothesis is tested. In this manner the consistency of the specific assumptions in regard to the particle content in the desert with the hypothesis of the gauge coupling unification is subjected to an experimental test. The well known spectacular success of this methodology is in differentiating between gauge coupling unification in supersymmetric and non–supersymmetric Grand Unified Theories [1]. The unification hypothesis is found not to be consistent with the low energy data, unless the minimal particle content is supersymmetric, or is modified in some other way. Our task then is to develop additional tools that can serve as similar useful probes of the desert.

1.1 Motivations for this work

In this paper we start applying this philosophy to another physical setting.

A different experimental observation - which also points toward the validity of the big desert scenario - is the existence of Ultra High Energy Cosmic Rays above the Greisen–Zatsepin–Kuzmin cutoff. A plausible explanation for the observation of such cosmic rays is the existence of supermassive metastable states with mass of the order $10^{12} - 10^{13}$GeV, and a lifetime that exceeds $10^{10}y$. The possibility that such states compose a substantial component of the dark matter as well as that they may explain the observation of UHECR has been discussed elsewhere. It has been further shown that realistic string models often give rise to states with precisely such properties [2].

The existence of such super–massive, slowly decaying states, may therefore serve as a probe of the grand desert. A plausible explanation of the observed showers in the UHECR is that the original supermassive decaying particle decays into strongly interacting particles which subsequently fragment into hadrons [3]. This hypothesis

therefore needs the relevant fragmentation functions at the energy scale of the originally decaying particle. These functions, however, similarly to the case of the gauge couplings considered in much of the literature on unification, are extracted from experiments at the currently accessible (low) energy scales which are much below that of the decaying particle. It is obvious that this points toward the use of the renormalization group (RG) evolution. However, this evolution, as well as the composition of the produced shower, depends on the assumptions made in regard to the composition of the spectrum in the desert. We conclude that similarly to the gauge coupling unification methodology, the evolution of the fragmentation functions by utilizing the renormalization group extrapolation, and the subsequent implementation in the analysis of the UHECR hadronic showers, can serve as a tool that differentiates between different assumptions on the very high energy spectrum.

With these motivations in mind, here we develop the instruments to evolve the fragmentation functions in supersymmetric QCD up to a high energy scale. In particular, in this paper we present for the first time the structure of the supersymmetric DGLAP (Exact Supersymmetric DGLAP or ESAP) equations in the timelike region. We solve them numerically for all flavours and introduce various combinations of non-singlet matrix equations to reach this result. We then study the impact of the new evolution assuming a common scale for susy breaking and restoration, parameterized by the mass of the superpartners, here assumed to be mass degenerate.

1.2 Step Approximations

Given the long stretch it takes to proceed with the analysis of the susy evolution, a topic of numerical complexity in its own, the applications to cosmic rays of our work will be presented in a companion paper that will follow shortly. We also have decided to address issues related to the fragmentation region of $N = 1$ QCD starting from the "low energy" end, since nothing is known of these functions at any scale. The term "low energy" (the results we discuss here are obtained in the $10^3 - 10^8$ GeV energy range) - from the point of view of collider phenomenology - is a misnomer, but it is not in the context of high energy cosmic ray physics. There is also another more direct reason for limiting our analysis to this range. We have discovered some features of the RG evolution which require a special care at such large energies. We find -in our numerical studies- the onset of an instability in the evolution in the singlet sector of the fragmentation which requires an independent investigation. It is not clear to us, at this point, whether this instability is an intrinsic limitation of the algorithm used in the numerical implementation or if the perturbative expansion needs a resummation. At such large scales this last option remains open. We should also mention that we work in "x" space, and this might be a limitation. We hope to return to this issue in the near future.

The analysis of fragmentation functions of Susy QCD is a topic of remarkable phenomenological interest both for collider phenomenology and in the astroparticle

context. While - recently - a detailed analysis of the supersymmetric evolution of the parton distributions of Susy QCD has been presented [4, 5, 6], the study of the evolution of the supersymmetric fragmentation functions is still missing. Of particular interest is the study of a combined QCD/SQCD evolution with intermediate regions in the evolution characterized by partial supersymmetry (SAP) or exact supersymmetry (ESAP) [5]. It is well known that a matching between these regions is possible with specific boundary conditions. These boundary conditions should come from some deeper understanding of the way in which supersymmetry is broken and restored as we run into the different stages of the renormalization group evolution. In a first approximation, however, it is possible to assume that the regular QCD distributions (or fragmentation) functions are continuous at each intermediate region, thereby neglecting threshold effects which can't be inferred from first principles. As we cross any supersymmetric region, starting, for instance, from the end of the regular QCD evolution, it is possible to assume that supersymmetric distributions and fragmentation functions are generated radiatively. We recall that a similar modeling -which neglects possible effects of higher twist at the thresholds- is well spread in the case of ordinary QCD.

2 Initial/Final State Scaling Violations

2.1 The Spacelike Evolution

The first analysis of the spacelike evolution was carried out in ref.[7], where simple models -obtained from the analysis of the first 2 moments - of the supersymmetric parton distributions were also presented. A complete strategy to solve these equations and the strategy to generate supersymmetric scaling violations in N=1 QCD was put forward in Refs. [4, 5]. In $N = 1$ QCD gluons have partners called gluinos (here denoted by λ) and left- and right-handed quarks have complex scalar partners (squarks) which we denote as $\tilde{q_L}$ and $\tilde{q_R}$ with $\tilde{q} = \tilde{q}_L + \tilde{q}_R$ (for left-handed and right-handed squarks respectively).

The interaction between the elementary fields are described by the $SU(3)$ color gauge invariant and supersymmetric Lagrangian

$$\begin{aligned}
&\mathcal{L} = -\frac{1}{4} G^a_{\mu\nu} G^{\mu\nu}_a + \frac{1}{2} \bar{\lambda}_a \left(i \not{D} \right) \lambda_a \\
&+ i \bar{q}_i \not{D} q_i + D_\mu \tilde{q}_R D^\mu \tilde{q}^R + D_\mu \tilde{q}_L D^\mu \tilde{q}_L + i g \sqrt{2} \left(\bar{\lambda^a}_R \tilde{q}^\dagger_{iL} T^a q_{Li} + \bar{\lambda^a}_L \tilde{q}^\dagger_{iR} T^a q_{Ri} - \texttt{h. c.} \right) \\
&- \frac{1}{2} g^2 \left(\tilde{q}^\dagger_{Li} T^a \tilde{q}_{Li} - \tilde{q}^\dagger_{Ri} T^a \tilde{q}^\dagger_{Ri} \right)^2 + \texttt{mass terms},
\end{aligned} \tag{1}$$

where a runs over the adjoint of the color group and i denotes the flavours.

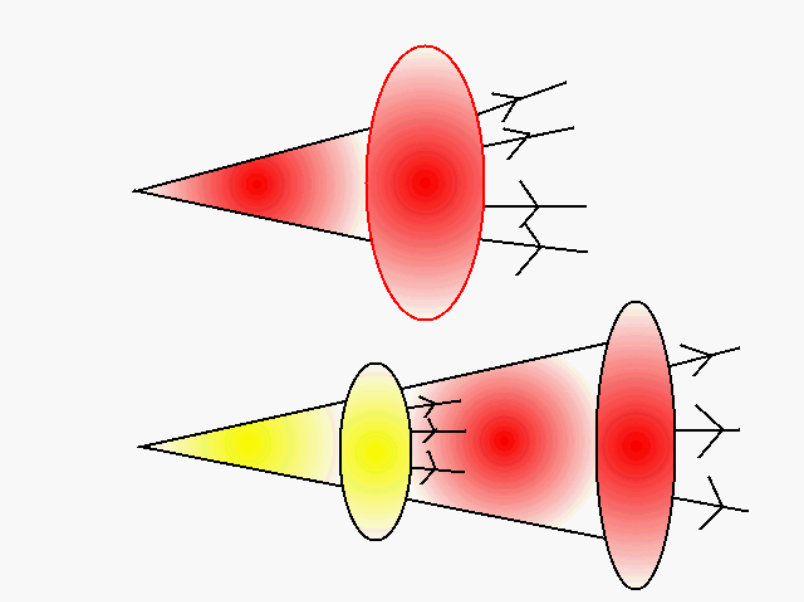

Figure 1: An illustration of the regular versus a mixed supersymmetric evolution

$\tilde{q}_{iR}$ are the supersymmetric partners of right-handed quarks q_{iR} and $\tilde{q}_{iL}$ are those of the left-handed quarks q_{iL}.

We remind here that in actual phenomenological applications, it is useful to extract the light-cone dynamics -or parton model picture- of supersymmetric collisions by invoking a factorization of the cross section into hard and soft contributions. Fragmentation functions appear in this context. An integral part of this analysis is the use of renormalization group equations -susy DGLAP- which resum the logarithmic scaling violations and evolve distributions functions and fragmentation functions to the appropriate factorization scale.

These studies require the matrix of the anomalous dimensions (for all the moments), or of the corresponding Altarelli-Parisi (DGLAP) kernels. We recall that the leading order anomalous dimensions are known [8, 7] both for a partial susy evolution and for the exact one.

2.2 The Timelike Evolution

In this work we focus our attention on the evolution of fragmentation functions in the context of exact supersymmetry, with coupled gluons and squarks. Fig. 1 summarizes the basic strategy of our work. The figure at the top depicts a regular evolution (a one-phase evolution), while the one at the bottom illustrates a mixed QCD/SQCD evolution (a two-phase evolution). The first stage is supersymmetric, the second one is regular. In the first stage all the partons (susy and not susy) are massless, in the second one only quark and gluons survive. At the end of the first stage the

supersymmetric partners are extinct, but their presence at the higher scales is saved in the boundary conditions for the quarks and gluons fragmentation functions, when the second stage of the evolution starts.

Within the approximation implied by the use of a pure SQCD evolution, no missing E_t events are allowed along the development of the supersymmetric cascade, since electroweak and flavour mixing effects are not included. Their inclusion is still an open chapter even in (QCD) Monte Carlo event generators for the final state.

The ladder structure of the supersymmetric showers in the leading logarithmic approximation can be easily pictured in terms of symmetric doubling of lines of regular QCD ladders in all the possible allowed cases. Showers can be equally initiated by $q\ \bar{q}$ pairs, gluon pairs, gluino pairs or squark pairs. The supersymmetric transition (i.e. those involving supersymmetric partners) stop (see Fig. 1 (bottom)) once the supersymmetry breaking scale $M_\lambda = M_{\tilde{q}}$ is reached.

Similarly to the QCD case, in the case of exact $N = 1$ supersymmetry we define singlet and non-singlet fragmentation functions $D_f^h(x, Q^2)$. They describe the amplitude for a parton of type f to fragment into a hadron h as a function of the Bjorken variable x (fractional energy of the fragment) and initial energy Q. Their operatorial definition is similar to that of ordinary parton distributions. The evolution equations for these functions are similar to the standard DGLAP equations, but with transposed kernel matrix ($P \to P^T$). In leading order the analytic continuation (from the spacelike or DIS evolution to the timelike evolution) is straightforward, while some complications appear to next-to-leading order. They involve a breaking of the Drell-Yan-Levy relation, which appears to be violated at parton level [9]. Since our analysis is in the leading logarithmic approximation, we will not consider these aspects in our work any further.

The equations for the timelike evolution are given by

$$\begin{aligned}
\frac{d}{d\log(Q^2)} D_g^h(x,Q^2) &= \frac{\alpha_s}{2\pi}\left(P_{gg}\otimes D_g^h + P_{\lambda g}\otimes D_\lambda^h + P_{qg}\otimes \sum_i \left(D_{q_i}^h + D_{\bar{q}_i}^h\right)\right. \\
&\qquad \left. + P_{\tilde{q}g}\otimes \sum_{i=1}^{n_f} (\tilde{q}_{iL} + \tilde{q}_{iR} + \bar{\tilde{q}}_{iL} + \bar{\tilde{q}}_{iR})\right) \qquad (2)\\
\frac{d}{d\log(Q^2)} D_\lambda^h(x,Q^2) &= \frac{\alpha_s}{2\pi}\left(P_{g\lambda}\otimes D_g^h + P_{\lambda\lambda}\otimes D_\lambda^h + P_{q\lambda}\otimes \sum_i \left(D_{q_i}^h + D_{\bar{q}_i}^h\right)\right. \\
&\qquad \left. + P_{\tilde{q}\lambda}\otimes \sum_{i=1}^{n_f} (\tilde{q}_{iL} + \tilde{q}_{iR} + \bar{\tilde{q}}_{iL} + \bar{\tilde{q}}_{iR})\right) \qquad (3)\\
\frac{d}{d\log(Q^2)} D_{q_i}^h(x,Q^2) &= \frac{\alpha_s}{2\pi}\left(\frac{1}{2n_f} P_{gq}\otimes D_g^h + \frac{1}{2n_f} P_{\lambda q}\otimes D_\lambda^h + P_{\tilde{q}q}\otimes \left(D_{\tilde{q}_{iL}}^h + D_{\tilde{q}_{iR}}^h\right)\right. \\
&\qquad \left. + P_{qq}\otimes D_{q_i}^h\right) \qquad (4)
\end{aligned}$$

$$\begin{aligned}
\frac{d}{d\log(Q^2)}D^h_{\tilde{q}_{iL}}(x,Q^2) &= \frac{\alpha_s}{2\pi}\left(\frac{1}{4n_f}P_{g\tilde{q}}\otimes D^h_g+\frac{1}{4n_f}P_{\lambda\tilde{q}}\otimes D^h_\lambda+\frac{1}{2}P_{q\tilde{q}}\otimes D^h_{q_i}\right.\\
&\qquad \left.+P_{\tilde{q}\tilde{q}}\otimes D^h_{\tilde{q}_{iL}}\right) \qquad (5)\\
\frac{d}{d\log(Q^2)}D^h_{\tilde{q}_{iR}}(x,Q^2) &= \frac{\alpha_s}{2\pi}\left(\frac{1}{4n_f}P_{g\tilde{q}}\otimes D^h_g+\frac{1}{4n_f}P_{\lambda\tilde{q}}\otimes D^h_\lambda+\frac{1}{2}P_{q\tilde{q}}\otimes D^h_{q_i}\right.\\
&\qquad \left.+P_{\tilde{q}\tilde{q}}\otimes D^h_{\tilde{q}_{iR}}\right) \qquad (6)
\end{aligned}$$

In the following we will use the short-hand notation

$$D^h_{\tilde{q}_i}(x,Q^2)\equiv D^h_{\tilde{q}_{iL}}(x,Q^2)+D^h_{\tilde{q}_{iR}}(x,Q^2) \qquad (7)$$

to denote the fragmentation functions of squarks of flavour i at a fractional energy x and momentum Q. It is also convenient to separate the equations, as usual, into singlet and non singlet sectors using the definitions

$$\begin{aligned}
D^h_{q_V}(x,Q^2) &\equiv \sum_{i=1}^{n_f}\left(D^h_{q_i}(x,Q^2)-D^h_{\bar{q}_i}(x,Q^2)\right),\\
&\equiv D^h_{q_{NS}}\\
D^h_{\tilde{q}_V}(x,Q^2) &= \sum_{i=1}^{n_f}\left(D^h_{\tilde{q}_i}(x,Q^2)-D^h_{\bar{\tilde{q}}_i}(x,Q^2)\right)\\
&\equiv D^h_{\tilde{q}_{NS}}(x,Q^2)\\
D_{q^+}(x,Q^2) &\equiv \sum_{i=1}^{n_f}\left(D^h_{q_i}(x,Q^2)+D^h_{\bar{q}_i}(x,Q^2)\right)\\
D^h_{\tilde{q}^+}(x,Q^2) &\equiv \sum_{i=1}^{n_f}\left(D^h_{\tilde{q}_i}(x,Q^2)+D^h_{\bar{\tilde{q}}_i}(x,Q^2)\right). \qquad (8)
\end{aligned}$$

The non singlet equations are

$$\begin{aligned}
Q^2\frac{d}{dQ^2}Dq_V(x,Q^2) &= \frac{\alpha(Q^2)}{2\pi}\left(P_{qq}\otimes D^h_{q_V}+P_{\tilde{q}q}\otimes D_{q_{\tilde{V}}}\right)\\
Q^2\frac{d}{dQ^2}D_{\tilde{q}_V}(x,Q^2) &= \frac{\alpha(Q^2)}{2\pi}\left(P_{q\tilde{q}}\otimes D^h_{q_V}+P_{\tilde{q}\tilde{q}}\otimes D^h_{q_{\tilde{V}}}\right), \qquad (9)
\end{aligned}$$

and the singlet matrix equations, which mix q_V and $\tilde{q}_V$ with the gluons and the gluinos

$$Q^2\frac{d}{dQ^2}\left[\begin{array}{c} D_g^h(x,Q^2) \\ D_\lambda^h(x,Q^2) \\ D_{q^+}^h(x,Q^2) \\ D_{\tilde{q}^+}^h(x,Q^2) \end{array}\right] = \left[\begin{array}{cccc} P_{gg} & P_{g\lambda} & P_{gq} & P_{g\tilde{q}} \\ P_{\lambda g} & P_{\lambda\lambda} & P_{\lambda q} & P_{\lambda\tilde{q}} \\ P_{qg} & P_{q\lambda} & P_{qq} & P_{q\tilde{q}} \\ P_{\tilde{q}g} & P_{\tilde{q}\lambda} & P_{\tilde{q}q} & P_{\tilde{q}\tilde{q}} \end{array}\right]^T \otimes \left[\begin{array}{c} D_g^h(x,Q^2) \\ D_\lambda^h(x,Q^2) \\ D_{q^{(+)}}^h(x,Q^2) \\ D_{\tilde{q}^{(+)}}^h(x,Q^2) \end{array}\right]. \qquad (10)$$

where "T" indicates the matrix transposed. To solve for all the flavours, it is convenient to introduce the linear combinations

$$\begin{aligned} \chi_i(x,Q^2) &= D_{q_i^{(+)}}^h - \frac{1}{n_f} D_{q^{(+)}}^h \\ \tilde{\chi}_i(x,Q^2) &= D_{\tilde{q}_i^{(+)}}^h - \frac{1}{n_f} D_{\tilde{q}^{(+)}}^h \end{aligned} \qquad (11)$$

and the additional singlet equations

$$\begin{aligned} Q^2\frac{d}{dQ^2} D_{q_i^{(-)}}(x,Q^2) &= \frac{\alpha(Q^2)}{2\pi}\left(P_{qq}\otimes D_{q_i^{(-)}}^h + P_{\tilde{q}q}\otimes D_{\tilde{q}_i{}^{(-)}}\right) \\ Q^2\frac{d}{dQ^2} D_{\tilde{q}_i^{(-)}}(x,Q^2) &= \frac{\alpha(Q^2)}{2\pi}\left(P_{q\tilde{q}}\otimes D_{q_i^{(-)}}^h + P_{\tilde{q}\tilde{q}}\otimes D_{\tilde{q}_i^{(-)}}^h\right) \end{aligned} \qquad (12)$$

and

$$\begin{aligned} Q^2\frac{d}{dQ^2} D_{\chi_i}^h(x,Q^2) &= \frac{\alpha(Q^2)}{2\pi}\left(P_{qq}\otimes D_{\chi_i}^h + P_{\tilde{q}q}\otimes D_{\tilde{\chi}_i}^h\right) \\ Q^2\frac{d}{dQ^2} D_{\tilde{\chi}_i}^h(x,Q^2) &= \frac{\alpha(Q^2)}{2\pi}\left(P_{q\tilde{q}}\otimes D_{\chi_i}^h + P_{\tilde{q}\tilde{q}}\otimes D_{\tilde{\chi}_i}^h\right). \end{aligned} \qquad (13)$$

The general flavour decomposition is obtained by solving the singlet equations for $D_{q^{(+)}}^h$ and $D_{\tilde{q}^{(+)}}^h$, then solving the non-singlet equations for $D_{q_i^{(-)}}^h$ and $D_{\tilde{q}_i^{(+)}}^h$ and for $D_{\chi_i}^h$ and $D_{\tilde{\chi}_i}^h$. The fragmentation functions of the various flavours are extracted using the linear combinations

$$\begin{aligned} D_{q_i}^h &= \frac{1}{2}\left(D_{q_i^{(-)}}^h + D_{\chi_i}^h + \frac{1}{n_f} D_{q^{(+)}}^h\right) \\ D_{\bar{q}_i}^h &= -\frac{1}{2}\left(D_{q_i^{(-)}}^h - D_{\chi_i}^h - \frac{1}{n_f} D_{q^{(+)}}^h\right) \end{aligned} \qquad (14)$$

and

$$
\begin{aligned}
D^h_{\tilde{q}_i} &= \frac{1}{2}\left(D^h_{\tilde{q}_i^{(-)}} + D^h_{\tilde{\chi}_i} + \frac{1}{n_f} D^h_{\tilde{q}^{(+)}}\right) \\
D^h_{\bar{\tilde{q}}_i} &= -\frac{1}{2}\left(D^h_{\tilde{q}_i^{(-)}} - D^h_{\tilde{\chi}_i} - \frac{1}{n_f} D^h_{\tilde{q}^{(+)}}\right)
\end{aligned}
\tag{15}
$$

to identify the various flavour components.

There are simple ways to calculate the kernel of the susy DGLAP evolution by a simple extension of the usual methods. The changes are primarily due to color factors. There are also some basic supersymmetric relations which have to be satisfied [4]. They are generally broken in the case of decoupling. We recall that the supersymmetric version of the β function is given at two-loop level by

$$
\begin{aligned}
\beta_0^S &= \frac{1}{3}\left(11\, C_A - 2\, n_f - 2\, n_\lambda\right) \\
\beta_1^S &= \frac{1}{3}\left(34\, C_A^2 - 10\, C_A\, n_f - 10\, C_A\, n_\lambda - 6\, C_F\, n_f - 6\, C_\lambda\, n_\lambda\right)
\end{aligned}
\tag{16}
$$

where n_f is the number of flavours and for Majorana gluinos $n_\lambda = C_A$.

The ordinary running of the coupling is replaced by its supersymmetric running

$$
\frac{\alpha^S(Q_0^2)}{2\pi} = \frac{2}{\beta_0^S}\frac{1}{\ln(Q^2/\Lambda^2)}\left(1 - \frac{\beta_1^S}{\beta_0^S}\frac{\ln\ln(Q^2/\Lambda^2)}{\ln(Q^2/\Lambda^2)} + O(\frac{1}{\ln^2(Q^2/\Lambda^2)})\right). \tag{17}
$$

The kernels are modified both in their coupling ($\alpha \to \alpha^S$) and in their internal structure (Casimirs, color factors, etc.) when moving from the QCD case to the SQCD case. In order to illustrate the approach that we are going to follow in our analysis of the fragmentation functions within a mixed SQCD/QCD evolution, we recall the strategy employed in Refs. [4, 5] to generate the ordinary supersymmetric distribution functions.

In Ref. [5] for scaling violations affecting the initial state were introduced 3 regions:

- 1) the QCD region, described by ordinary QCD (Altarelli Parisi or AP) ;
- 2) an intermediate supersymmetric region with coupled gluinos and decoupled squarks (partially supersymmetric AP or SAP);
- 3) the N=1 region (exact supersymmetric AP or ESAP).

The basic idea was to generate these distributions *radiatively* as usually done in QCD for the gluons, for instance, using the fact that the matrix of the anomalous dimensions is not-diagonal. The most general sequence of evolutions (denoted AP-SAP-ESAP in [5]) is described by the arrays $(Q_i, Q_f)_{AP} - (Q_i, Q_f)_{SAP} - (Q_i, Q_f)_{ESAP}$,

with $Q_{f,AP} = Q_{i,SAP} = m_{2\lambda}$ and $Q_{f,SAP} = Q_{i,ESAP} = m_{\tilde{q}}$. In this work we limit our analysis to a simpler AP-ESAP evolution and we run the DGLAP equations *back* starting from known QCD fragmentation functions - for which various sets are available in the literature [11] - up to an intermediate supersymmetric scale. From this point on (up in energy) we switch on the ESAP evolution of fragmentation functions. As we run the equations upward, supersymmetric fragmentation functions are generated. The boundary values of the low energy (QCD) functions at the supersymmetry scale $m_{2\lambda}$ set the initial condition for the (backward) supersymmetric running up to the final scale. In simple terms: we reach the mountain from the valley, and cross a fence along the way.

In general, if we split the intermediate susy scale into 2 sectors $m_{\tilde{q}} << m_{2\lambda}$ (ESAP-SAP-AP evolution) in this (general) case the solution is built by sewing the three regions as

$$\begin{aligned}
\begin{bmatrix} D^h_{q_V}(x,Q^2) \\ D^h_{\tilde{q}_V}(x,Q^2) \end{bmatrix} &= \begin{bmatrix} D^h_{q_V}(x,Q_0^2) \\ 0 \end{bmatrix} + \int_{Q_0^2}^{m^2_{2\lambda}} d\,\log\, Q^2\, P^{T,NS}_{AP}(x,\alpha(Q^2)) \otimes \begin{bmatrix} D^h_{q_V}(x,Q^2) \\ 0 \end{bmatrix} \\
&+ \int_{m^2_{2\lambda}}^{m^2_{\tilde{q}}} d\,\log Q^2 P^{T,NS}_{SAP}(x,\alpha^S(Q^2)) \otimes \begin{bmatrix} D^h_{q_V}(x,Q^2) \\ 0 \end{bmatrix} \\
&+ \int_{m^2_{2\lambda}}^{Q^2_f} d\,\log Q^2\, P^{T,NS}_{ESAP}(x,\alpha^{ES}(Q^2)) \otimes \begin{bmatrix} D^h_{q_V}(x,Q^2) \\ D^h_{\tilde{q}^V}(x,Q^2) \end{bmatrix}
\end{aligned} \tag{18}$$

in the non singlet and

$$\begin{aligned}
\begin{bmatrix} D^h_G(x,Q^2_f) \\ D^h_\lambda(x,Q^2) \\ D^h_{q^+}(x,Q^2) \\ D^h_{\tilde{q}^+}(x,Q^2) \end{bmatrix} &= \begin{bmatrix} D^h_G(x,Q^2_f) \\ 0 \\ D^h_{q^+}(x,Q^2_f) \\ 0 \end{bmatrix} + \int_{Q_0^2}^{m^2_{2\lambda}} d\,\log\, Q^2\, P^{NS}_{T,AP}(x,\alpha(Q^2)) \otimes \begin{bmatrix} D^h_G(x,Q^2_f) \\ 0 \\ D^h_{q^+}(x,Q^2) \\ 0 \end{bmatrix} \\
&+ \int_{m^2_{2\lambda}}^{m^2_{\tilde{q}}} d\,\log Q^2 P^{NS}_{T,SAP}(x,\alpha^S(Q^2)) \otimes \begin{bmatrix} D^h_G(x,Q^2_f) \\ D^h_\lambda(x,Q^2) \\ D^h_{q^+}(x,Q^2) \\ 0 \end{bmatrix} \\
&+ \int_{m^2_{2\lambda}}^{Q^2_f} d\,\log Q^2\, P^{NS}_{T,ESAP}(x,\alpha^{ES}(Q^2)) \otimes \begin{bmatrix} D^h_G(x,Q^2_f) \\ D^h_\lambda(x,Q^2) \\ D^h_{q^+}(x,Q^2) \\ D^h_{\tilde{q}^+}(x,Q^2) \end{bmatrix}
\end{aligned} \tag{19}$$

for the singlet solution. The zero entries in the arrays for some of the distributions are due to the boundary conditions, since all the supersymmetric partners are generated, in this model, by the evolution.

The general structure of the algorithms that solves these equations is summarized below. We start from the non singlet sector and then proceed to the singlet. From now on, to simplify our notation, we will omit at times the index "h" from the fragmentation functions when obvious. We define $D_{q^{NS}}(x,Q^2) = (D_{q_V}(x,Q^2), D_{\tilde{q}_V}(x,Q^2))^T$ and $DA_n(x) = \left(DA_n^{q_V}, DA_n^{\tilde{q}_V}\right)^T$ and introduce the ansatz

$$D_{q^{NS}}(x,Q^2) = \sum_{n=0}^{n_0} \frac{A_n(x)}{n!} \log^n \left(\frac{\alpha(Q^2)}{\alpha(Q_0^2)}\right), \tag{20}$$

where n_0 is an integer at which we stop the iteration, which usually ranges up to 20. The first coefficient of the recursion is determined by the initial condition

$$DA_0(x) = U(x) \otimes D_q^{NS}(x,Q_0^2), \tag{21}$$

where

$$\begin{aligned} U_1(x) &\equiv \begin{bmatrix} \delta(1-x) & 0 \\ 0 & 0 \end{bmatrix} \\ U_{1\,2}(x) &\equiv \begin{bmatrix} \delta(1-x) & 0 \\ 0 & \delta(1-x) \end{bmatrix}. \end{aligned} \tag{22}$$

The recursion relations are given by

$$DA_{n+1}(x) = -\frac{2}{\beta_0} P_{AP}^{T,NS} \otimes DA_n(x) \tag{23}$$

The solution in the first (DGLAP) region at the first matching scale $m_{2\lambda}$ is given by

$$D_{q^{NS}}(x,m_{2\lambda}) = \sum_{n=0}^{n_0} \frac{DA_n^{AP}(x)}{n!} \log^n \left(\frac{\alpha({m_{2\lambda}}^2)}{\alpha(Q_0^2)}\right). \tag{24}$$

At the second stage the (partial) supersymmetric coefficients are given by (S is a short form of SAP)

$$\begin{aligned} DA_0^{S,NS}(x) &= U(x) \otimes D_q(x, m_{2\lambda^2}) \\ DA_{n+1}^{S,NS}(x) &= -\frac{2}{\beta_0^S} P_S^{T,NS}(x) \otimes DA_n^{S,NS}(x). \end{aligned} \tag{25}$$

We construct the boundary condition for the next stage of the evolution using the intermediate solution

$$D_q(x,Q^2) = \sum_{n=0}^{n_0} \frac{DA_n^S(x)}{n!} \left(\frac{\alpha(Q^2)}{\alpha({m_{2\lambda}}^2)}\right). \tag{26}$$

evaluated at the next threshold $m_{2\lambda}$.

$$D_q(x,Q^2) = \sum_{n=0}^{n_0} \frac{DA_n^S(x)}{n!} \log\left(\frac{\alpha(Q^2)}{\alpha({m_{2\lambda}}^2)}\right). \tag{27}$$

The final solution is constructed using the recursion relations

$$\begin{aligned} DA_0^{ES}(x) &= U(x) \otimes q(x, m_{\tilde{q}}) \\ DA_{n+1}^{ES}(x) &= -\frac{2}{\beta^{ES}} P_{ES}^{NS}(x) \otimes DA_n^{ES}(x) \end{aligned} \tag{28}$$

The final solution is written as

$$\begin{aligned} D_{q^{NS}}(x,Q^2) &= D_{q^{NS}}(x,Q_0^2) + \sum_{n=1}^{n_0} \frac{DA_n(x)}{n!} \log\left(\frac{\alpha({m_{2\lambda}}^2)}{\alpha(Q_0^2)}\right) + \sum_{n=1}^{n_0} \frac{DA_n^S(x)}{n!} \log\left(\frac{\alpha^S(m_{\tilde{q}}^2)}{\alpha^S({m_{2\lambda}}^2)}\right) \\ &+ \sum_{n=1}^{n_0} \frac{DA_n^{ES}(x)}{n!} \log\left(\frac{\alpha^{ES}(Q_f^2)}{\alpha^{ES}({m_{\tilde{q}}}^2)}\right) \end{aligned} \tag{29}$$

As we have already mentioned above, in the analysis presented below the two susy scales will be collapsed into one ($m_{2\lambda}$).

3 QCD Evolution of the Fragmentation Functions

As we have already mentioned, the timelike and the spacelike evolution, in leading order, are essentially the same. The singlet kernels are just the transposed of the kernels describing the evolution of the parton distributions. The ordinary QCD kernels, in leading order, are given by

$$\begin{aligned} P_{qq,NS}^{(0)} &= C_F \left(\frac{1+x^2}{1-x}\right)_+ \\ &= C_F \left(\frac{2}{(1-x)_+} - 1 - x + \frac{3}{2}\,\delta(1-x)\right) \\ P_{qq}^{(0)}(x) &= P_{qq,NS}^{(0)} \\ P_{qg}^{(0)}(x) &= n_f \left(x^2 + (1-x)^2\right) \\ P_{gq}^{(0)}(x) &= C_F \frac{1+(1-x)^2}{x} \\ P_{gg}^{(0)}(x) &= 2N_c \left(\frac{1}{(1-x)_+} + \frac{1}{x} - 2 + x(1-x)\right) + \frac{\beta_o}{2}\delta(1-x) \end{aligned} \tag{30}$$

with $\beta_0 = 11/3\,C_A - 4/3\,T_R\,n_f$ being the first coefficient of the QCD β-function and $T_R = 1/2$. n_f is the numbers of flavours. The equations for the fragmentation functions in QCD are given by

$$\begin{aligned}
\frac{d}{d\log(Q^2)} D^h_{q_i}(x,Q^2) &= \frac{\alpha(Q^2)}{2\pi}\left(P_{qq}\otimes D^h_{q_i} + \frac{1}{2n_f}P_{gq}\otimes D^h_g\right) \\
\frac{d}{d\log(Q^2)} D^h_g(x,Q^2) &= \frac{\alpha(Q^2)}{2\pi}\left(P_{qg}\otimes \sum_i \left(D^h_{q_i} + D^h_{\bar{q}_i}\right) + P_{gg}\otimes D^h_g\right)
\end{aligned} \tag{31}$$

and, as usual, can be decomposed into a non-singlet and a singlet sector

$$Q^2\frac{d}{dQ^2} D^h_{q_i^{(-)}}(x,Q^2) = \frac{\alpha(Q^2)}{2\pi} P_{qq,\,NS}(x,\alpha(Q^2))\otimes D^h_{q_i^{(-)}}(x,Q^2) \tag{32}$$

for the non-singlet distributions and

$$\frac{d}{d\log(Q^2)}\begin{pmatrix} D^h_{q^{(+)}}(x,Q^2) \\ D^h_g(x,Q^2)\end{pmatrix} = \begin{pmatrix} P_{qq} & P_{gq} \\ P_{qg} & P_{gg}\end{pmatrix}\otimes\begin{pmatrix} D^h_{q^{(+)}}(x,Q^2) \\ D^h_g(x,Q^2)\end{pmatrix} \tag{33}$$

for the singlet sector, where

$$D^h_{q_i^{(-)}}(x,Q^2) = D^h_{q_i} - D^h_{\bar{q}_i}. \tag{34}$$

A fast strategy to solve these equations, as discussed in [4], where a complete leading order evolution has been implemented, is to solve the recursion relations numerically. In the timelike case -that we are considering- these relations are obtained as linear combinations of the spacelike ones. We get

$$\begin{aligned}
DA^{q_i^{(-)}}_{n+1} &= -4\frac{C_F}{\beta_0}\int_x^1 \frac{dy}{y}\frac{yDA^{q_i^{(-)}}_n(y) - xDA^{q_i^{(-)}}_n(x)}{y-x} - 4\frac{C_F}{\beta_0}\log(1-x)DA^{q_i^{(-)}}_n(x) \\
&\quad +2\frac{C_F}{\beta_0}\int_x^1 \frac{dy}{y}\,(1+z)\,DA^{q_i^{(-)}}_n(y) - 3\frac{C_F}{\beta_0}DA^{q_i^{(-)}}_n(x) \\
DA^{q^{(-)}}_{n+1} &= -4\frac{C_F}{\beta_0}\int_x^1 \frac{dy}{y}\frac{yDA^{q^{(-)}}_n(y) - xDA^{q^{(-)}}_n(x)}{y-x} - 4\frac{C_F}{\beta_0}\log(1-x)DA^{q^{(-)}}_n(x) \\
&\quad +2\frac{C_F}{\beta_0}\int_x^1 \frac{dy}{y}\,(1+z)\,DA^{q^{(-)}}_n(y) - 3\frac{C_F}{\beta_0}DA^{q^{(-)}}_n(x).
\end{aligned} \tag{35}$$

A similar expansion is set up for the non-singlet variable $\chi_i = q_i^{(+)} - 1/n_f\ q^{(+)}$

$$\begin{aligned} DA_{n+1}^{\chi_i} &= -4\frac{C_F}{\beta_0}\int_x^1 \frac{dy}{y}\frac{yDA_n^{\chi_i}(y) - xDA_n^{\chi_i}(x)}{y-x} - 4\frac{C_F}{\beta_0}\log(1-x)DA_n^{\chi_i}(x) \\ &\quad +2\frac{C_F}{\beta_0}\int_x^1 \frac{dy}{y}\,(1+z)\,DA_n^{\chi_i}(y) - 3\frac{C_F}{\beta_0}DA_n^{\chi_i}(x). \end{aligned} \tag{36}$$

Similarly, the singlet equations generate recursion relations of the form

$$\begin{aligned} DA_{n+1}^{q^{(+)}}(x) &= -4\frac{C_F}{\beta_0}\int_x^1 \frac{dy}{y}\frac{yDA_n^{q^{(+)}}(y) - xDA_n^{q^{(+)}}(x)}{y-x} - 4\frac{C_F}{\beta_0}\log(1-x)DA_n^{q^{(+)}}(x) \\ &\quad +2\frac{C_F}{\beta_0}\int_x^1 \frac{dy}{y}\,(1+z)\,DA_n^{q^{(+)}}(y) - 3\frac{C_F}{\beta_0}DA_n^{q^{(+)}}(x) \\ &\quad -2\frac{C_F}{\beta_0}\int_x^1 \frac{dy}{y}\frac{1+(1-z)^2}{z}DA_n^{g}(y) \\ DA_{n+1}^{g}(x) &= -4\frac{C_A}{\beta_0}\int_x^1 \frac{dy}{y}\frac{yDA_n^{g}(y) - xDA_n^{g}(x)}{y-x} - 4\frac{C_A}{\beta_0}\log(1-x)DA_n^{g}(x) \\ &\quad -2\frac{n_f}{\beta_0}\int_x^1 \frac{dy}{y}\left(z^2+(1-z)^2\right)DA_n^{q^{(+)}}(y) - DA_n^{g}(x) \\ &\quad -4\frac{C_A}{\beta_0}\int_x^1 \frac{dy}{y}\left(\frac{1}{z} - 2 + z(1-z)\right)DA_n^{g}(y). \end{aligned} \tag{37}$$

The coefficients of the various flavours both for $D_{q_i}^h$ and $D_{\bar{q}_i}^h$ are then obtained from the relations

$$\begin{aligned} DA_n^{q_i} &= \frac{1}{2}\left(DA_n^{\chi_i} + \frac{1}{n_f}DA_n^{q_i^{(-)}}\right) \\ DA_n^{\bar{q}_i} &= \frac{1}{2}\left(DA_n^{\chi_i} - \frac{1}{n_f}DA_n^{q_i^{(-)}}\right) \end{aligned} \tag{38}$$

4 The ESAP ($N = 1$ QCD) Fragmentation

Moving to $N = 1$ QCD, we introduce recursion relations for appropriate linear combinations of non-singlet fragmentation functions

$$\begin{aligned} DA_{n+1}^{\chi_i} &= -4\frac{C_F}{\beta_0}\int_x^1 \frac{dy}{y}\frac{yDA_n^{\chi_i}(y) - xDA_n^{\chi_i}(x)}{y-x} - 4\frac{C_F}{\beta_0}\log(1-x)DA_n^{\chi_i}(x) \\ &\quad -2\frac{C_F}{\beta_0}DA_n^{\chi_i}(x) - 2\frac{C_F}{\beta_0}\int_x^1 \frac{dy}{y}zDA_n^{\tilde{\chi}_i}(y) + 2\frac{C_F}{\beta_o}\int_x^1 \frac{dy}{y}\,(1+z)\,DA_n^{\chi_i}(y) \end{aligned} \tag{39}$$

$$
\begin{aligned}
DA^{\tilde{\chi}_i}_{n+1} &= -4\frac{C_F}{\beta_0}\int_x^1 \frac{dy}{y}\frac{yDA^{\tilde{\chi}_i}_n(y) - xDA^{\tilde{\chi}_i}_n(x)}{y-x} - 4\frac{C_F}{\beta_0}\log(1-x)DA^{\tilde{\chi}_i}_n(x) \\
&\quad -2\frac{C_F}{\beta_0}DA^{\tilde{\chi}_i}_n(x) - 2\frac{C_F}{\beta_0}\int_x^1 \frac{dy}{y} z DA^{\chi_i}_n(y) + 2\frac{C_F}{\beta_o}\int_x^1 \frac{dy}{y}\,(1+z)\,DA^{\tilde{\chi}_i}_n(y)
\end{aligned}
\tag{40}
$$

and two similar non-singlet equations for $D^h_{q_i^{(-)}}$ and $D^h_{\tilde{q}_i^{(-)}}$

$$
\begin{aligned}
DA^{q_i^{(-)}}_{n+1} &= -4\frac{C_F}{\beta_0}\int_x^1 \frac{dy}{y}\frac{yDA^{q_i^{(-)}}_n(y) - xDA^{q_i^{(-)}}_n(x)}{y-x} - 4\frac{C_F}{\beta_0}\log(1-x)DA^{q_i^{(-)}}_n(x) \\
&\quad -2\frac{C_F}{\beta_0}DA^{q_i^{(-)}}_n(x) - 2\frac{C_F}{\beta_0}\int_x^1 \frac{dy}{y} z DA^{\tilde{q}_i^{(-)}}_n(y) + 2\frac{C_F}{\beta_o}\int_x^1 \frac{dy}{y}\,(1+z)\,DA^{q_i^{(-)}}_n(y)
\end{aligned}
\tag{41}
$$

$$
\begin{aligned}
DA^{\tilde{q}_i^{(-)}}_{n+1} &= -4\frac{C_F}{\beta_0}\int_x^1 \frac{dy}{y}\frac{yDA^{\tilde{q}_i^{(-)}}_n(y) - xDA^{\tilde{q}_i^{(-)}}_n(x)}{y-x} - 4\frac{C_F}{\beta_0}\log(1-x)DA^{\tilde{q}_i^{(-)}}_n(x) \\
&\quad -2\frac{C_F}{\beta_0}DA^{\tilde{q}_i^{(-)}}_n(x) - 2\frac{C_F}{\beta_0}\int_x^1 \frac{dy}{y} z DA^{q_i^{(-)}}_n(y) + 2\frac{C_F}{\beta_o}\int_x^1 \frac{dy}{y}\,(1+z)\,DA^{\tilde{q}_i^{(-)}}_n(y).
\end{aligned}
\tag{42}
$$

Analogous equations are satisfied by the combinations $D^h_{q^{(-)}}$ and $D^h_{\tilde{q}^{(-)}}$ by replacing in (41) and (42) $D^h_{q_i^{(-)}} \to D^h_{q^{(-)}}$ and $D^h_{\tilde{q}_i^{(-)}} \to D^h_{\tilde{q}^{(-)}}$.

Moving to the singlet sector we obtain

$$
\begin{aligned}
DA^g_{n+1}(x) &= -4\frac{C_A}{\beta_0}\int_x^1 \frac{dy}{y}\frac{yDA^g_n(y) - xDA^g_n(x)}{y-x} - 4\frac{C_A}{\beta_0}\log(1-x)DA^g_n(x) - DA^g_n(x) \\
&\quad +2\frac{C_A}{\beta_0}\int_x^1 \frac{dy}{y}\,(1+z)\,DA^g_n(y) - 2\frac{C_A}{\beta_0}\int_x^1 \frac{dy}{y}\left(\frac{2}{z}+z-2\right)DA^g_n(y) \\
&\quad +2\frac{C_A}{\beta_0}\int_x^1 \frac{dy}{y}\left(z^2+(1-z)^2\right)DA^g_n(y) - 2\frac{n_f}{\beta_0}\int_x^1 \frac{dy}{y}\left(z^2+(1-z)^2\right)DA^q_n(y) \\
&\quad -2\frac{C_A}{\beta_0}\int_x^1 \frac{dy}{y}\left(z^2+(1-z)^2\right)DA^\lambda_n(y) - 4\frac{n_f}{\beta_0}\int_x^1 \frac{dy}{y}\,z\,(1-z)\,DA^{\tilde{q}}_n(y)
\end{aligned}
\tag{43}
$$

$$
DA^\lambda_n(x) = -2\frac{C_A}{\beta_0}\int_x^1 \frac{dy}{y}\left(\frac{2}{z}+z-2\right)DA^g_n(y) - 4\frac{C_A}{\beta_0}\int_x^1 \frac{dy}{y}\frac{DA^\lambda_n(y) - xDA^\lambda_n(x)}{y-x}
$$

$$-4\frac{C_A}{\beta_0}\log(1-x)DA_n^{\lambda}(x)+2\frac{C_A}{\beta_0}\int_x^1\frac{dy}{y}\,(1+z)\,DA_n^{\lambda}(y)-DA_n^{\lambda}(x)$$
$$-2\frac{n_f}{\beta_0}\int_x^1\frac{dy}{y}\,(1-z)\,DA_n^{q}(y)-2\frac{n_f}{\beta_0}\int_x^1\frac{dy}{y}zDA_n^{\tilde{q}}(y) \qquad (44)$$

$$\begin{aligned}DA_{n+1}^{q^{(+)}}(x) &= -2\frac{C_F}{\beta_0}\int_x^1\frac{dy}{y}\left(\frac{2}{z}+z-2\right)DA_n^{g}(y)-2\frac{C_F}{\beta_0}\int_x^1\frac{dy}{y}\,(1-z)\,DA_n^{\lambda}(y)\\ &-4\frac{C_F}{\beta_0}\int_x^1\frac{dy}{y}\frac{yDA_n^{q^{(+)}}(y)-xDA_n^{q^{(+)}}(x)}{y-x}-4\frac{C_F}{\beta_0}\log(1-x)DA_n^{q^{(+)}}(x)\\ &+2\frac{C_F}{\beta_0}\int_x^1\frac{dy}{y}\,(1+z)\,DA_n^{q^{(+)}}(y)-2\frac{C_F}{\beta_0}DA_n^{q^{(+)}}(x)-2\frac{C_F}{\beta_0}\int_x^1\frac{dy}{y}zDA_n^{\tilde{q}^{(+)}}(y)\end{aligned} \qquad (45)$$

$$\begin{aligned}DA_{n+1}^{\tilde{q}^{(+)}}(x) &= -2\frac{C_F}{\beta_0}\int_x^1\frac{dy}{y}\left(\frac{2}{z}-2\right)DA_n^{g}(y)-2\frac{C_F}{\beta_0}\int_x^1\frac{dy}{y}\left(DA_n^{\lambda}(x)-DA_n^{\tilde{q}^{(+)}}(y)\right)\\ &-4\frac{C_F}{\beta_0}\int_x^1\frac{dy}{y}\frac{yDA_n^{\tilde{q}}(y)-xDA_n^{\tilde{q}}(x)}{y-x}+4\frac{C_F}{\beta_0}\int_x^1\frac{dy}{y}DA_n^{\tilde{q}}(y)\\ &-4\frac{C_F}{\beta_0}\log(1-x)DA_n^{\tilde{q}^{(+)}}(y)-2\frac{C_F}{\beta_0}DA_n^{\tilde{q}^{(+)}}(x)\end{aligned} \qquad (46)$$

where $z \equiv x/y$.

5 Numerical Results

As an illustration of the procedure we adopt in our studies, let's consider the decay of a hypothetical massive state of mass 1 TeV into supersymmetric partons. The decay can proceed, for instance, through a regular $q\bar{q}$ channel and a shower is developed starting from the quark pair. The $N = 1$ DGLAP equation describes in the leading logarithmic approximation the evolution of the shower which accompanies the pair, and we are interested in studying the impact of the supersymmetry breaking scale (m_λ) on the fragmentation. In our runs we have chosen the initial set of Ref. [11]. The parameterizations are shown in the appendix just for illustrative purposes. In our analysis we focus on proton fragmentation functions. As in Ref. [11], we introduce the scaling variable

$$\bar{s} = \ln\frac{\ln\left(\mu^2/\Lambda^{(5)}_{\overline{\rm MS}}\right)}{\ln\left(\mu_0^2/\Lambda^{(5)}_{\overline{\rm MS}}\right)}. \qquad (47)$$

In LO we have $\Lambda^{(5)}_{\overline{\rm MS}} = 88$ MeV [11]. We use three different values for μ_0, namely [11]

$$\mu_0 \;=\; \begin{cases} \sqrt{2}\ \text{GeV}, & \text{if} \quad a = u,d,s,g \\ m(\eta_c) = 2.9788\ \text{GeV}, & \text{if} \quad a = c \\ m(\Upsilon) = 9.46037\ \text{GeV}, & \text{if} \quad a = b \end{cases} . \tag{48}$$

This leads to three different definitions of $\bar{s}$. For definiteness, we use the symbol $\bar{s}_c$ for charm and $\bar{s}_b$ for bottom along with $\bar{s}$ for the residual partons. We parameterize the f.f.'s as

$$D(x,\mu^2) = N x^\alpha (1-x)^\beta \left(1 + \frac{\gamma}{x}\right) \tag{49}$$

and express the coefficients N, α, β, and γ as polynomials in $\bar{s}$, $\bar{s}_c$, and $\bar{s}_b$. For $\bar{s} = \bar{s}_c = \bar{s}_b = 0$, the parameterizations agree with Eq. (2) of Ref. [11] in combination with the appropriate entries in Table 2 of that paper. The charm and bottom parameterizations must be put to zero by hand for $\bar{s}_c < 0$ and $\bar{s}_b < 0$, respectively.

Typical fragmentation functions in QCD involve final states with p, $\bar{p}$, $\pi^\pm, \pi^0$ and kaons $k^\pm$. We have included the relevant sets from ref. [11] that we have employed in our numerical analysis in an appendix. We refer to the original literature for a list of all the fragmentation sets. We have chosen an initial evolution scale of 10 GeV and varied both the mass of the susy partners (we assume for simplicity that these are all degenerate) and the final evolution scale. Since our concern is in establishing the impact of supersymmetric evolution and compare it to standard QCD evolution across large evolution intervals, we plot the initial fragmentation functions, the regularly evolved QCD functions and the SQCD/QCD evolved ones. The latter two are originated from the same low energy form of Ref. [11]. The figures show that the effects of supersymmetric evolution are small within the range described by the factorization scales Q_f and Q_i ($Q_f = 10^3$ GeV, $Q_i = 200$ GeV). We mention that Q_f is the starting scale (the highest scale) at which the decay of the supersymmetric partons starts. Q_i is fixed by the gluino/squark masses and coincides with them. It is possible to include in the evolution of the fragmentation functions also different thresholds associated with more complex spectra in which the susy partners are not degenerate. These effects are negligible. Threshold enhancements may require a more accurate treatment and will be discussed elsewhere, however we don't expect them to play any important role, especially since we are interested in very extended renormalization group runnings. Fig. 2 shows the initial condition for the up quark fragmentation function. We have chosen $Q_0 = 10$ GeV, extrapolated from collider data in Ref. [11] in their global analysis. The evolution of this function follows QCD from this lowest scale up to a scale of 400 GeV ($m_{2\lambda}$). Above this scale we use the full $N = 1$ evolution. The initial fragmentation scale, here denoted by Q_f is 1 TeV. In general, the small-x (diffractive) region gets slightly enhanced. The highest scale is not large enough to allow a discrimination of susy effects from the non supersymmetric ones. The trend of the two evolved curves is similar. In Fig. 3 an analogous behaviour is found for the fragmentation functions of charm and strange

quarks. Again, small-x enhancements are seen, but regular and susy evolution are hardly distinguishable. The situation appears to be completely different for the gluon fragmentation functions (f.f's) (Fig. 4). The regular and the SQCD evolved f.f.'s differ largely in the diffractive region, and this clearly will show up in the spectrum of the primary protons if the decaying state has a supersymmetric content. As we raise the final evolution scale we start seeing more pronounced differences between regular and supersymmetric distributions. We have shown in Fig. 5 the squark f.f.'s for all the flavours and the one of the gluino for comparison. The scalar charm distribution appear to grow slightly faster then the remaining scalar ones. The gluino f.f. is still the fastest growing at small-x values.

In Figs. 6 and 7 this trend is quite evident for the quark and gluon fragmentation functions respectively. The latter is the distributions which remains by far the most sensitive to changes in the highest fragmentation scale. It is therefore very likely that the spectrum of final protons is substantially modified by this fast modifications of the gluon density. A sustained stability -as we raise the supersymmetric scale - of all the distributions is also noticed. In fact, in Fig. 8 we vary the gluino mass for a fixed final highest scale and notice a mild variation of the fragmentation function of the up quark. A similar behaviour is recorded in Fig. 9, where we compare the fragmentation functions of the up quark and of its superpartner at various m_λ's. The shape of the gluino density as a function of the the initial fragmentation scale is shown in Fig. 10. The growth appears to be fast and is rather pronounced. Fig. 11 finally illustrates the behaviour of f.f's of all types at a large initial fragmentation scale. In order to illustrate the different behaviours that the quark/squark sector has compared to the gluon/gluino sector, we have shown the f.f.'s for the b quark and the $\tilde{b}$ squark. Although all the functions get a small-x enhancement or are more supported in this x-region, the largest fragmentation appears to come from the gluon-gluino sector.

6 Conclusions

We have presented a first detailed study of the fragmentation functions of susy QCD in the leading logarithmic approximation and presented, for the first time, results for the f.f.'s of all the partons into protons within a radiatively generated model. Our analysis is motivated by the growing interest that high energy cosmic rays experiments will be receiving in the next several years from the astroparticle/high energy physics community. There are hints, from this work, that supersymmetric effects may affect substantially the fragmentation region and the spectra of the hadronic component of cosmic rays which is expected to play a dominant role as one approaches the GZK cutoff. Our analysis indicates that fragmentation probabilities are redistributed among the various open channel and have an impact on the spectrum of the primaries. Compared to initial state scaling violations where only a gluino of small mass seems to enhance the radiative structure of parton distributions [4, 5, 6], the cosmic ray

story clearly points to another direction. Given the very large energy available in the fragmentation region, and assuming a supersymmetry breaking scale of the order of 1 TeV, the f.f's, which control the multiplicities of the hadron component of the various channels are substantially affected by the presence of a supersymmetric scale at the highest energy. The natural question to ask is then: what are the distributions of supersymmetric partons in a decaying metastable state of very large mass prior to fragmentation? At such large scales, so far from the 1 TeV scale preferred by many standard supersymmetric arguments, the Renormalization Group strategy can be easily embraced to its fullest extent with sizeable consequences on the low energy end. On this and other related issues we hope to return in more detail in the near future.

Acknowledgements

We thank S. Sarkar and R. Toldra for discussions. C.C. and A.F. thank respectively the Theory Groups at Oxford and Lecce for hospitality. The work of C.C. is supported in part by INFN (iniziativa specifica BARI-21) and by MURST. The work of A.F. is supported by PPARC.

7 Appendix 1. Input Functions

For convenience we have included below the list of f.f.'s taken from Ref. [11] that we have used

- $D_u^{p/\bar{p}}(x,\mu^2) = 2D_d^{p/\bar{p}}(x,\mu^2)$:

$$\begin{aligned} N &= 0.40211 - 0.21633\bar{s} - 0.07045\bar{s}^2 + 0.07831\bar{s}^3 \\ \alpha &= -0.85973 + 0.13987\bar{s} - 0.82412\bar{s}^2 + 0.43114\bar{s}^3 \\ \beta &= 2.80160 + 0.78923\bar{s} - 0.05344\bar{s}^2 + 0.01460\bar{s}^3 \\ \gamma &= 0.05198\bar{s} - 0.04623\bar{s}^2 \end{aligned} \tag{50}$$

- $D_s^{p/\bar{p}}(x,\mu^2)$:

$$\begin{aligned} N &= 4.07885 - 2.97392\bar{s} - 0.92973\bar{s}^2 + 1.23517\bar{s}^3 \\ \alpha &= -0.09735 + 0.25834\bar{s} - 1.52246\bar{s}^2 + 0.77060\bar{s}^3 \\ \beta &= 4.99191 + 1.14379\bar{s} - 0.85320\bar{s}^2 + 0.45607\bar{s}^3 \\ \gamma &= 0.07174\bar{s} - 0.08321\bar{s}^2 \end{aligned} \tag{51}$$

- $D_c^{p/\bar{p}}(x,\mu^2)$:

$$N = 0.11061 - 0.07726\bar{s}_c + 0.05422\bar{s}_c^2 - 0.03364\bar{s}_c^3$$

$$\begin{aligned}
\alpha &= -1.54340 - 0.20804\bar{s}_c + 0.29038\bar{s}_c^2 - 0.23662\bar{s}_c^3 \\
\beta &= 2.20681 + 0.62274\bar{s}_c + 0.29713\bar{s}_c^2 - 0.21861\bar{s}_c^3 \\
\gamma &= 0.00831\bar{s}_c + 0.00065\bar{s}_c^2
\end{aligned} \tag{52}$$

- $D_b^{p/\bar{p}}(x,\mu^2)$:

$$\begin{aligned}
N &= 40.0971 - 123.531\bar{s}_b + 128.666\bar{s}_b^2 - 29.1808\bar{s}_b^3 \\
\alpha &= 0.74249 - 1.29639\bar{s}_b - 3.65003\bar{s}_b^2 + 3.05340\bar{s}_b^3 \\
\beta &= 12.3729 - 1.04932\bar{s}_b + 0.34662\bar{s}_b^2 - 1.34412\bar{s}_b^3 \\
\gamma &= -0.04290\bar{s}_b - 0.30359\bar{s}_b^2
\end{aligned} \tag{53}$$

- $D_g^{p/\bar{p}}(x,\mu^2)$:

$$\begin{aligned}
N &= 0.73953 - 1.64519\bar{s} + 1.01189\bar{s}^2 - 0.10175\bar{s}^3 \\
\alpha &= -0.76986 - 3.58787\bar{s} + 13.8025\bar{s}^2 - 13.8902\bar{s}^3 \\
\beta &= 7.69079 - 2.84470\bar{s} - 0.36719\bar{s}^2 - 2.21825\bar{s}^3 \\
\gamma &= 1.26515\bar{s} - 1.96117\bar{s}^2
\end{aligned} \tag{54}$$

8 Appendix 2. The Weights of the N=1 Kernels

We briefly recall the numerical strategy employed in this analysis. A more detailed description will be given elsewhere. We just mention that the radiative generation of supersymmetric distributions requires special accuracy since these scaling violations grow up very slowly. We define $\bar{P}(x) \equiv xP(x)$ and $\bar{A}(x) \equiv xA(x)$. We also define the convolution product

$$J(x) \equiv \int_x^1 \frac{dy}{y}\left(\frac{x}{y}\right) P\left(\frac{x}{y}\right) \bar{A}(y). \tag{55}$$

The integration interval in y at any fixed x-value is partitioned in an array of increasing points ordered from left to right $(x_0, x_1, x_2, ..., x_n, x_{n+1})$ with $x_0 \equiv x$ and $x_{n+1} \equiv 1$ being the upper edge of the integration region. One constructs a rescaled array $(x, x/x_n, ..., x/x_2, x/x_1, 1)$. We define $s_i \equiv x/x_i$, and $s_{n+1} = x < s_n < s_{n-1} < ...s_1 < s_0 = 1$. We get

$$J(x) = \sum_{i=0}^{N} \int_{x_i}^{x_{i+1}} \frac{dy}{y}\left(\frac{x}{y}\right) P\left(\frac{x}{y}\right) \bar{A}(y) \tag{56}$$

At this point we introduce the linear interpolation

$$\bar{A}(y) = \left(1 - \frac{y - x_i}{x_{i+1} - x_i}\right) \bar{A}(x_i) + \frac{y - x_i}{x_{i+1} - x_i} \bar{A}(x_{i+1}) \tag{57}$$

and perform the integration on each subinterval with a change of variable $y->x/y$ and replace the integral $J(x)$ with its discrete approximation $J_N(x)$ to get

$$\begin{aligned} J_N(x) &= \bar{A}(x_0)\frac{1}{1-s_1}\int_{s_1}^{1}\frac{dy}{y}P(y)(y-s_1) \\ &+ \sum_{i=1}^{N}\bar{A}(x_i)\frac{s_i}{s_i-s_{i+1}}\int_{s_{i+1}}^{s_i}\frac{dy}{y}P(y)(y-s_{i+1}) \\ &- \sum_{i=1}^{N}\bar{A}(x_i)\frac{s_i}{s_{i-1}-s_i}\int_{s_i}^{s_{i-1}}\frac{dy}{y}P(y)(y-s_{i-1}) \end{aligned} \tag{58}$$

with the condition $\bar{A}(x_{N+1})=0$. Introducing the coefficients $W(x,x)$ and $W(x_i,x)$, the integral is cast in the form

$$J_N(x) = W(x,x)\bar{A}(x) + \sum_{i=1}^{n} W(x_i,x)\bar{A}(x_i) \tag{59}$$

where

$$\begin{aligned} W(x,x) &= \frac{1}{1-s_1}\int_{s_1}^{1}\frac{dy}{y}(y-s_1)P(y), \\ W(x_i,x) &= \frac{s_i}{s_i-s_{i+1}}\int_{s_{i+1}}^{s_i}\frac{dy}{y}\left(y-s_{i+1}\right)P(y) \\ &- \frac{s_i}{s_{i-1}-s_i}\int_{s_i}^{s_{i-1}}\frac{dy}{y}\left(y-s_{i-1}\right)P(y). \end{aligned} \tag{60}$$

We recall that

$$\int_0^1 dx\frac{f(x)}{(1-x)_+} = \int_0^1 dy\frac{f(y)-f(1)}{1-y} \tag{61}$$

and that

$$\frac{1}{(1-x)_+}\otimes f(x) \equiv \int_x^1\frac{dy}{y}\frac{yf(y)-xf(x)}{y-x} + f(x)\log(1-x) \tag{62}$$

as can can be shown quite straightforwardly.

We also introduce the expressions

$$\begin{aligned} In_0(x) &= \frac{1}{1-s_1}\log(s_1)+\log(1-s_1) \\ Jn_i(x) &= \frac{1}{s_i-s_{i+1}}\left[\log\left(\frac{1-s_{i+1}}{1-s_i}\right)+s_{i+1}\log\left(\frac{1-s_i}{1-s_{i+1}}\frac{s_{i+1}}{s_i}\right)\right] \end{aligned}$$

$$
\begin{aligned}
Jnt_i(x) &= \frac{1}{s_{i-1}-s_i}\left[\log\left(\frac{1-s_i}{1-s_{i-1}}\right)+s_{i-1}\log\left(\frac{s_i}{s_{i-1}}\right)+s_{i-1}\left(\frac{1-s_{i-1}}{1-s_i}\right)\right], \quad i=2,3,..N \\
Jnt_1(x) &= \frac{1}{1-s_1}\log s_1.
\end{aligned}
\tag{63}
$$

Using the linear interpolation formula (57) we get the relation

$$
\begin{aligned}
\int_x^1 \frac{dy}{y}\frac{yA_n(y)-xA_n(x)}{y-x} &= -\log(1-x)A_n(x)+A_n(x)In_0(x) \\
&\quad +\sum_{i=1}^{N} A_n(x_i)\left(Jn_i(x)-Jnt_i(x)\right)
\end{aligned}
\tag{64}
$$

which has been used for a fast and accurate numerical implementation of the recursion relations.

References

[1] J. Ellis, S. Kelley and D.V. Nanopoulos, *Phys. Lett.* **B260** (1991) 131;
P. Langacker and M. Luo, *Phys. Rev.* **D44** (1991) 817;
U. Amaldi, W. de Boer and H. Füstenau, *Phys. Lett.* **B260** (1991) 447.

[2] C. Corianò, S. Chang and A.E. Faraggi, *Phys. Lett.* **B397** (1997) 76; *Nucl. Phys.* **B477** (1996) 65;
K. Benakli, J. Ellis and D.V. Nanopoulos, *Phys. Rev.* **D59** (1999) 047301; C. Corianò, A.E. Faraggi and M. Plümacher, OUTP-01-35P, to appear.

[3] For review and references see *e.g.*:
S. Sarkar, Plenary Talk at COSMO 99, hep-ph/0005256.

[4] C. Corianò Supersymmetric Scaling Violations. 1. An algorithm to solve the supersymmetric DGLAP evolution, hep-ph/0009227

[5] C. Corianò, Supersymmetric Scaling Violations 2. The general supersymmetric evolution , hep-ph/0102164

[6] C. Corianò, Distributions of $N = 1$ QCD, hep-ph/0101352

[7] C. Kounnas and D.A. Ross, Nucl. Phys. B214:317, (1983).

[8] I. Antoniadis, C. Kounnas and R. Lacaze, Nucl. Phys. B211:216, (1983).

[9] J. Blumlein, V. Ravindran and W.L. van Neerven Nucl.Phys.B586:349-381, (2000).

[10] K. Greisen, Phys. Rev. Lett. 16:748, (1966); G.T Zatsepin and V.A. Kuzmin, Sov. Phys. JETP Lett. 4:78 (1966).

[11] B.A. Kniehl, G. Kramer, B. Pötter, Nucl. Phys. B 582:514, (2000).

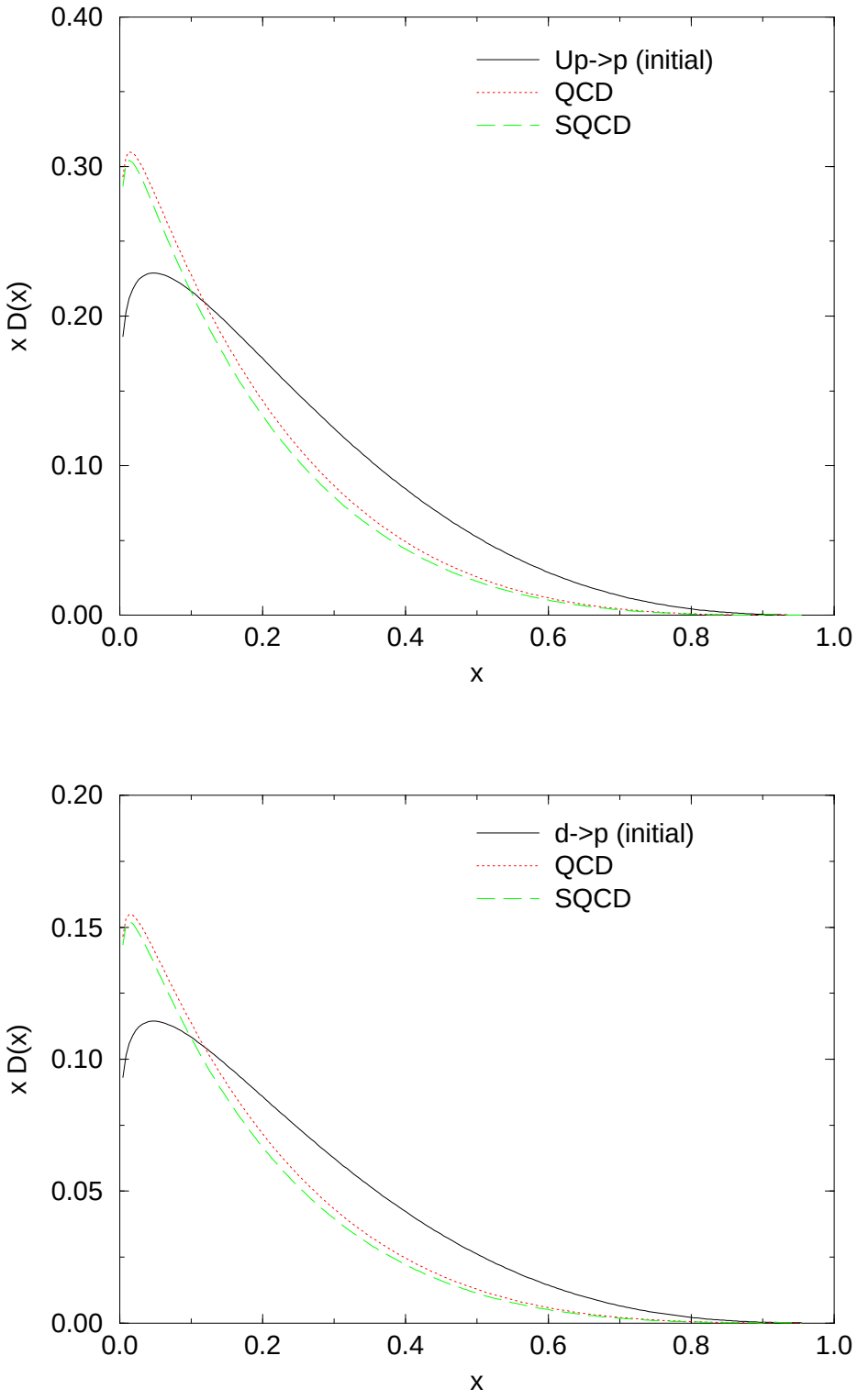

Figure 2: Fragmentation function for the up (top graph) and down quark (bottom graph) $xD_{u,d}^{p,\bar{p}}(x,Q^2)$ at the lowest scale (input) $Q_0 = 10$ GeV, and their QCD (or regular) and SQCD/QCD evolutions with Q_f =10^3 GeV.The susy fragmentation scale is chosen to be 200 GeV.

.

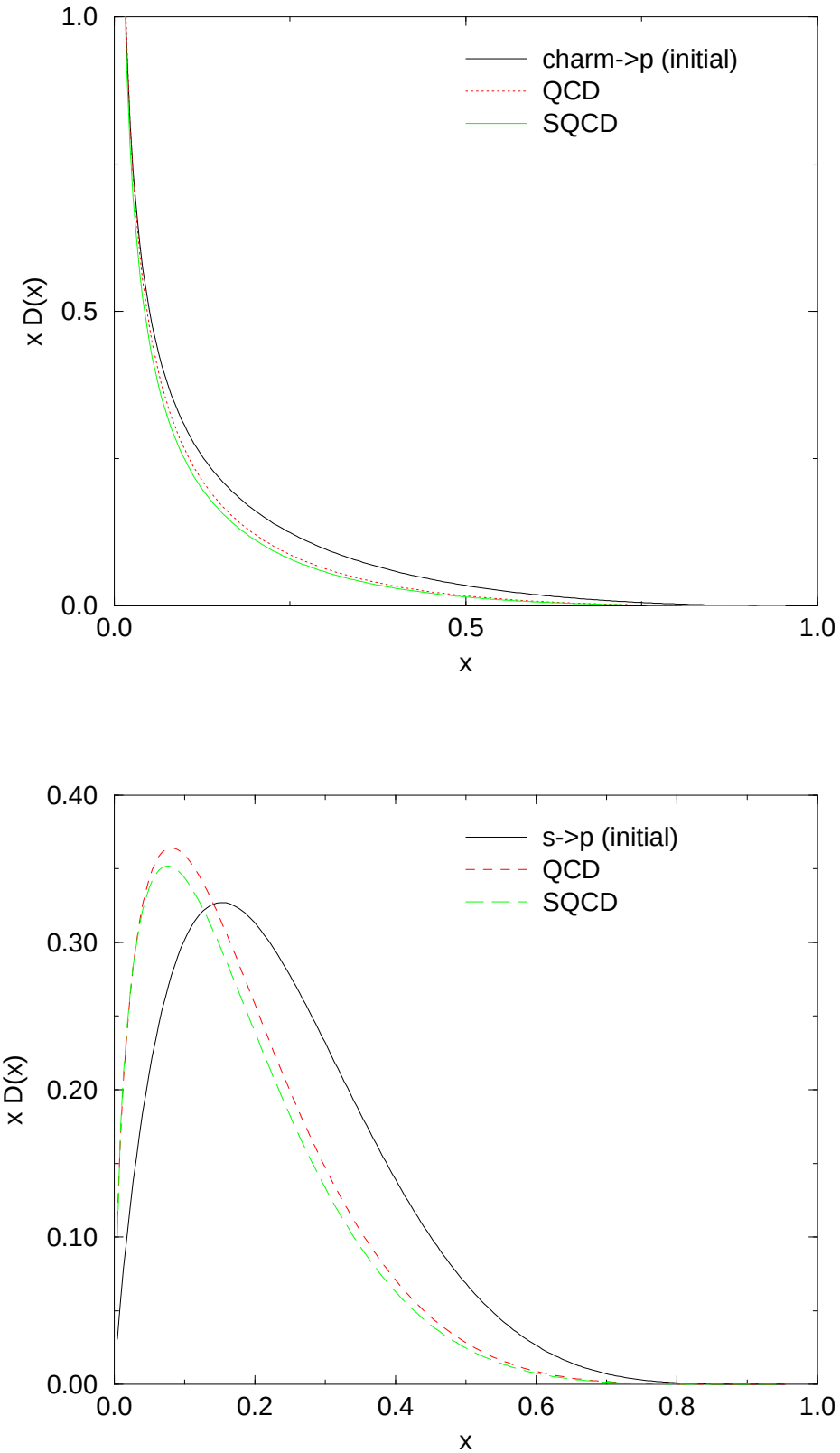

Figure 3: Fragmentation functions into protons of the charm and strange quarks $xD_{s,c}^{p,\bar{p}}(x,Q^2)$ at the lowest scale (input) $Q_0 = 10$ GeV, and its evolved QCD (regular) and SQCD/QCD evolutions with Q_f =10^3 GeV.The susy fragmentation scale is chosen to be 200 GeV.

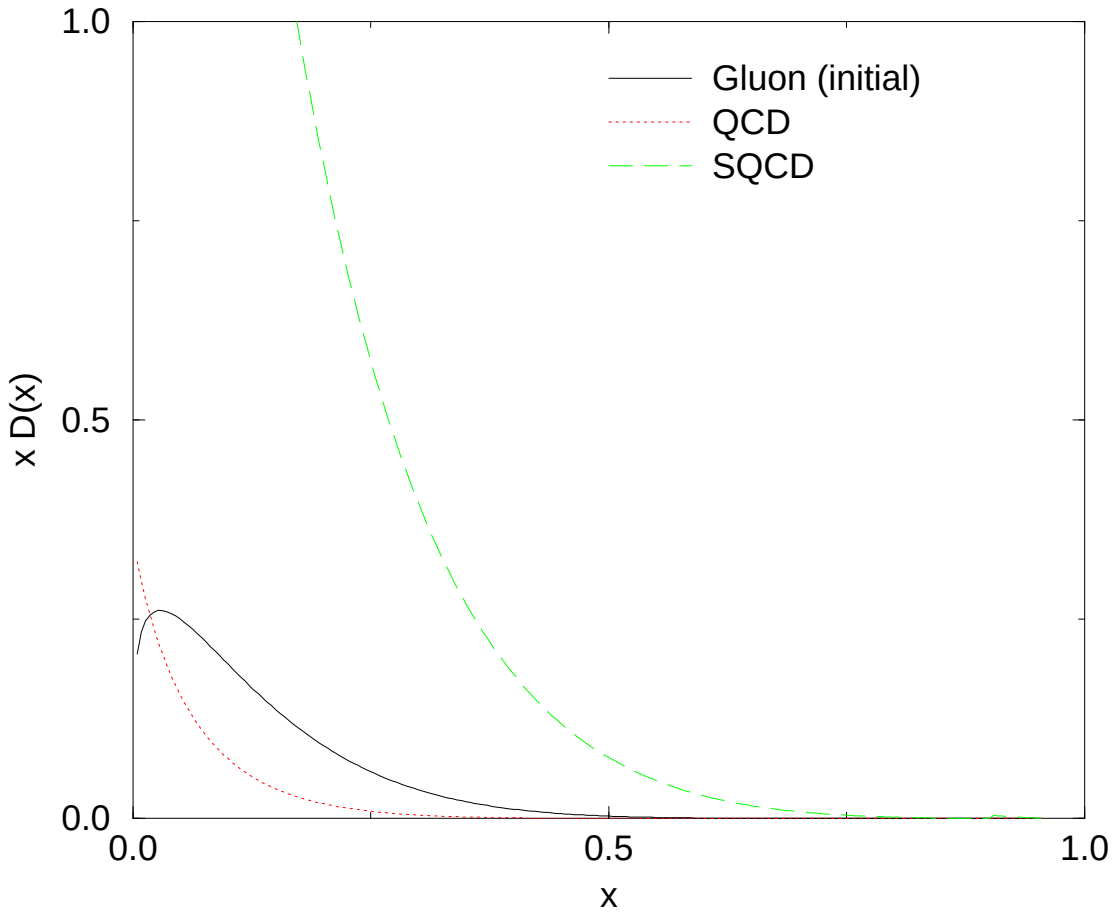

Figure 4: The gluon fragmentation function $xD_g^{p,\bar{p}}(x,Q^2)$ at the lowest scale (input) Q_0 = 10 GeV, and its evolved QCD (regular) and SQCD/QCD evolutions with Q_f =10^3 GeV.The susy fragmentation scale is chosen to be 200 GeV.

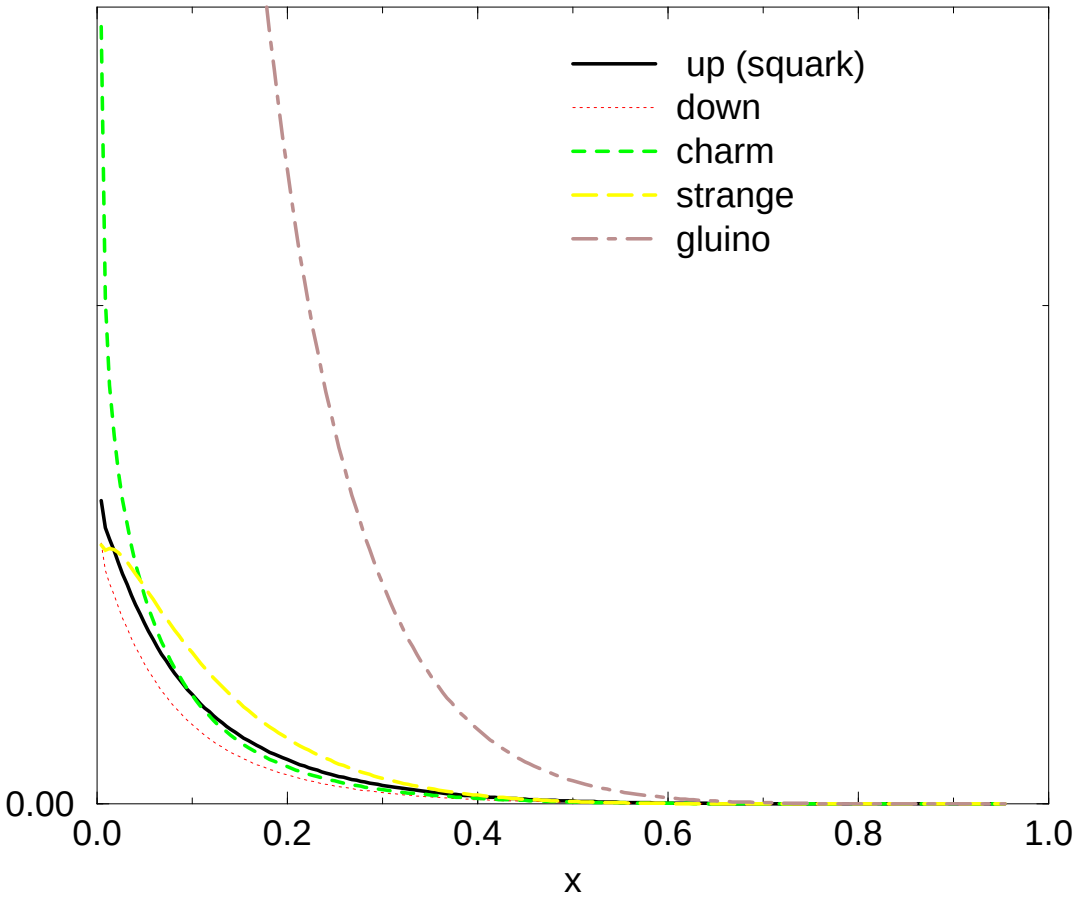

Figure 5: The fragmentation functions of squarks and gluino at the lowest scale (input) $Q_0 = 10$ GeV, with $Q_f = 10^3$ GeV and susy scale 200 GeV.

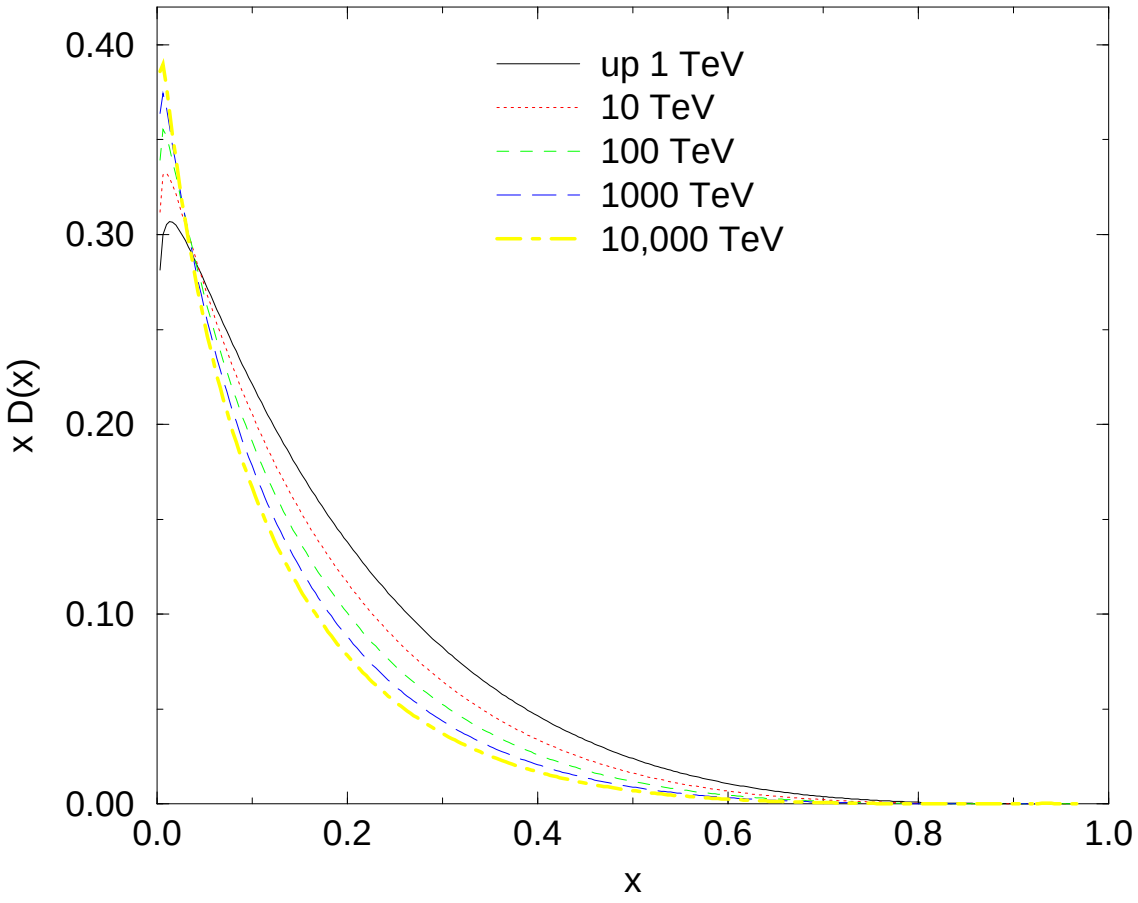

Figure 6: The up quark fragmentation function $xD_u^{p,\bar{p}}(x,Q^2)$ evolved with SQCD/QCD for varying final values of Q_f. The susy fragmentation scale is chosen to be 200 GeV.

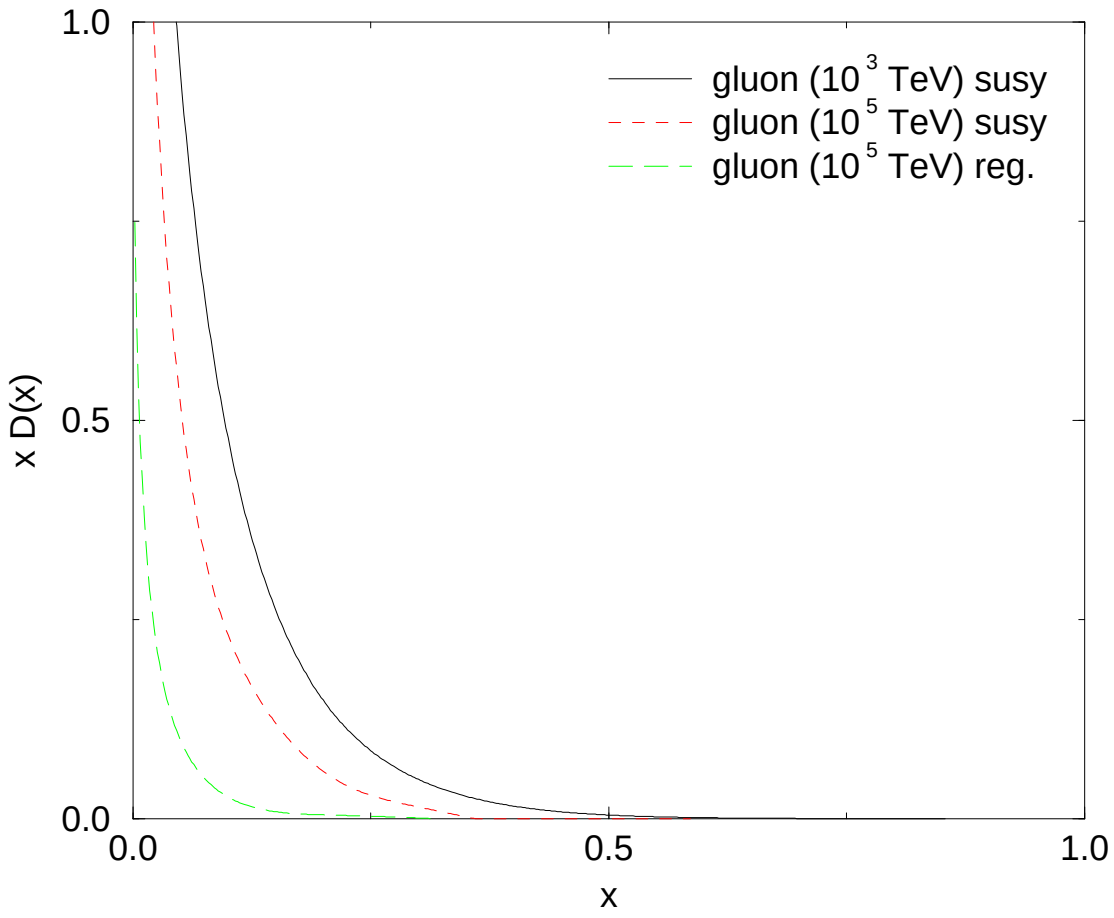

Figure 7: The gluon fragmentation function $xD_g^{p,\bar{p}}(x,Q^2)$ evolved regularly and according to SQCD/QCD for varying final values of Q_f. The susy fragmentation scale is chosen to be 200 GeV.

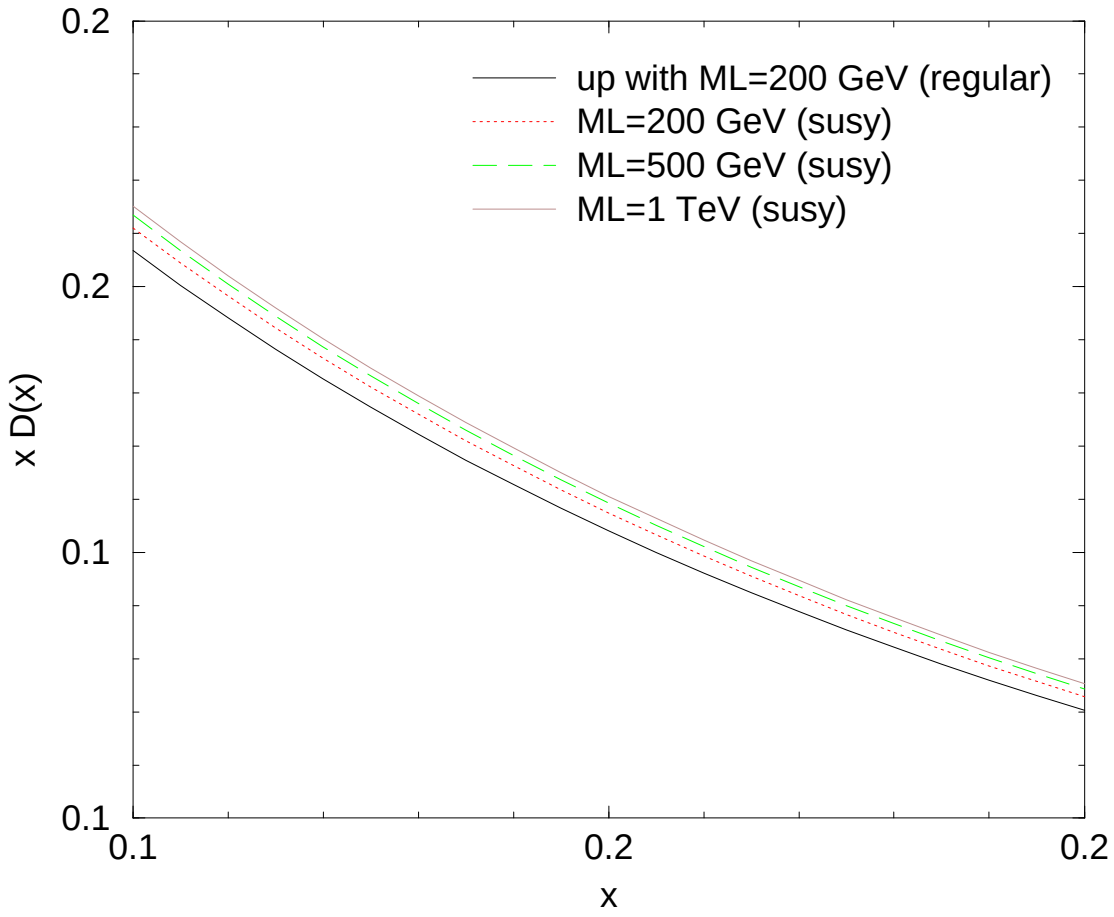

Figure 8: The up quark fragmentation function $xD_u^{p,\bar{p}}(x,Q^2)$ evolved regularly and according to SQCD/QCD for varying final values of the susy scale $m_{2\lambda}$ and $Q_f = 10^8$ GeV. The susy fragmentation scale is chosen to be 200 GeV.

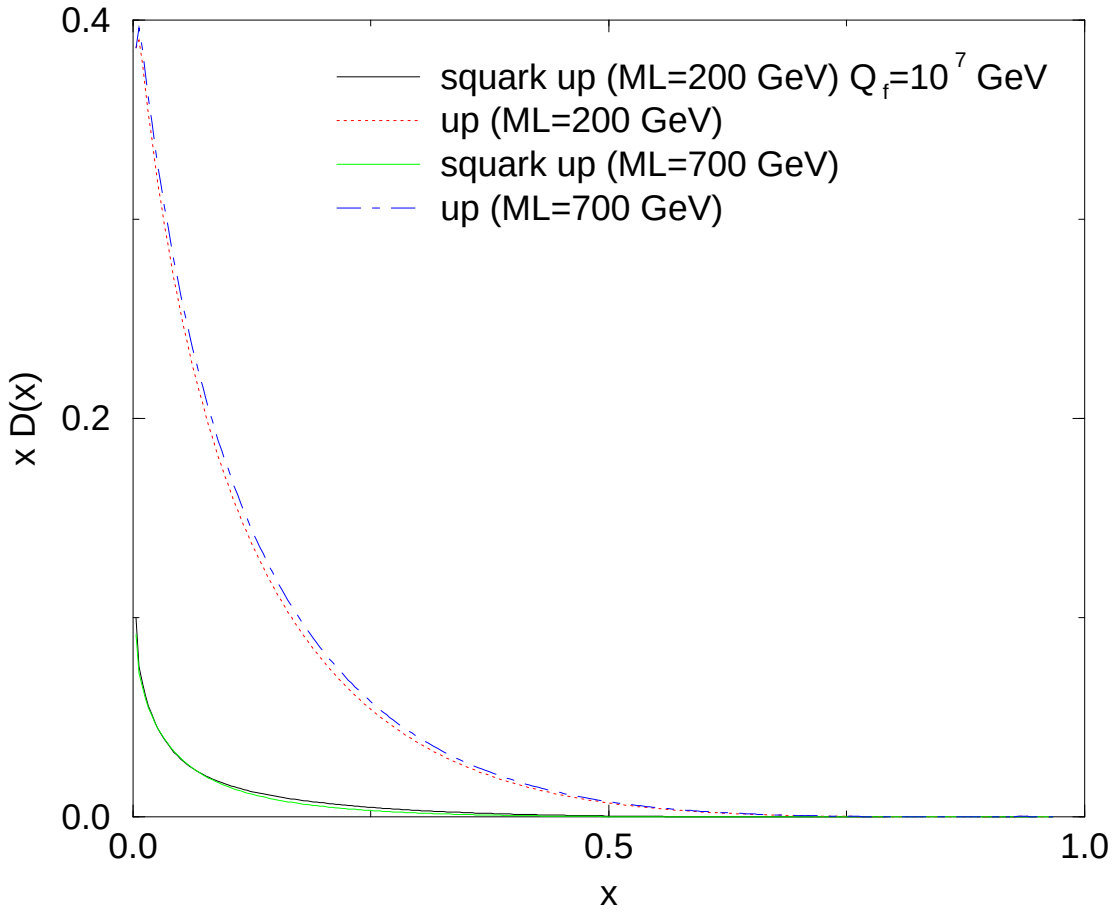

Figure 9: The quark and squark (up) fragmentation functions for a varying m_λ and a fixed large final scale $Q_f = 10^7$ GeV.

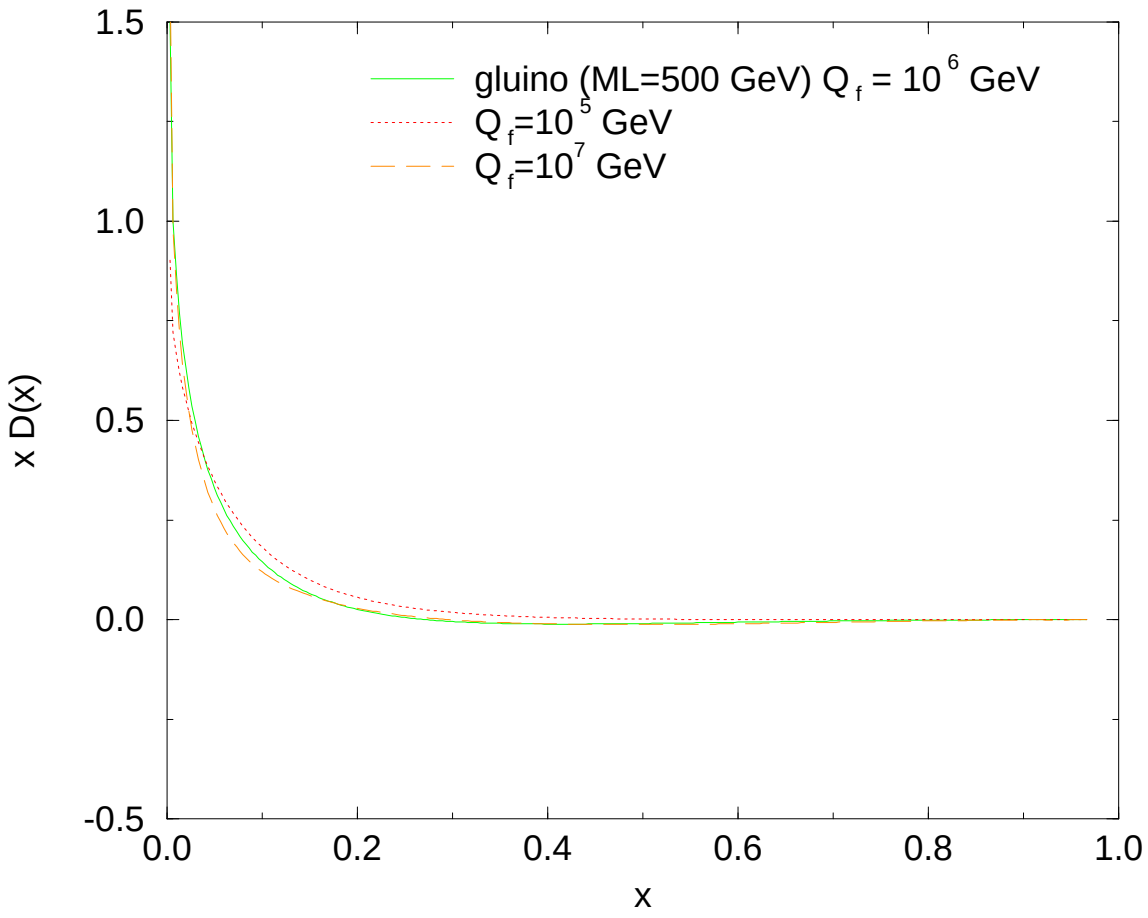

Figure 10: The gluino fragmentation function $xD_u^{p,\bar{p}}(x,Q^2)$ evolved in the region $500-Q_f$ GeV for different values of Q_f The susy fragmentation scale is chosen to be 500 GeV.

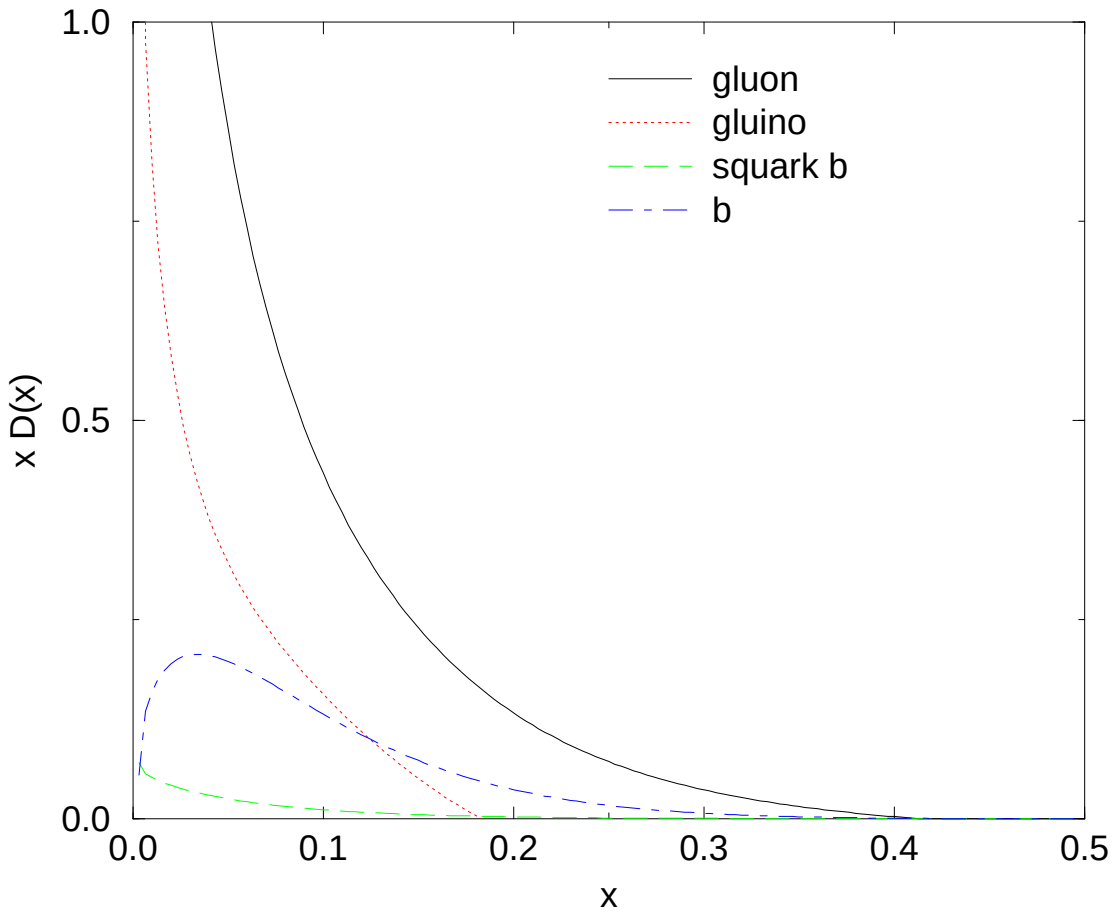

Figure 11: The quark and squark (bottom) fragmentation functions together with those of gluon and gluino for $m_\lambda = 500$ GeV and a fixed large final scale $Q_f = 10^7$ GeV.

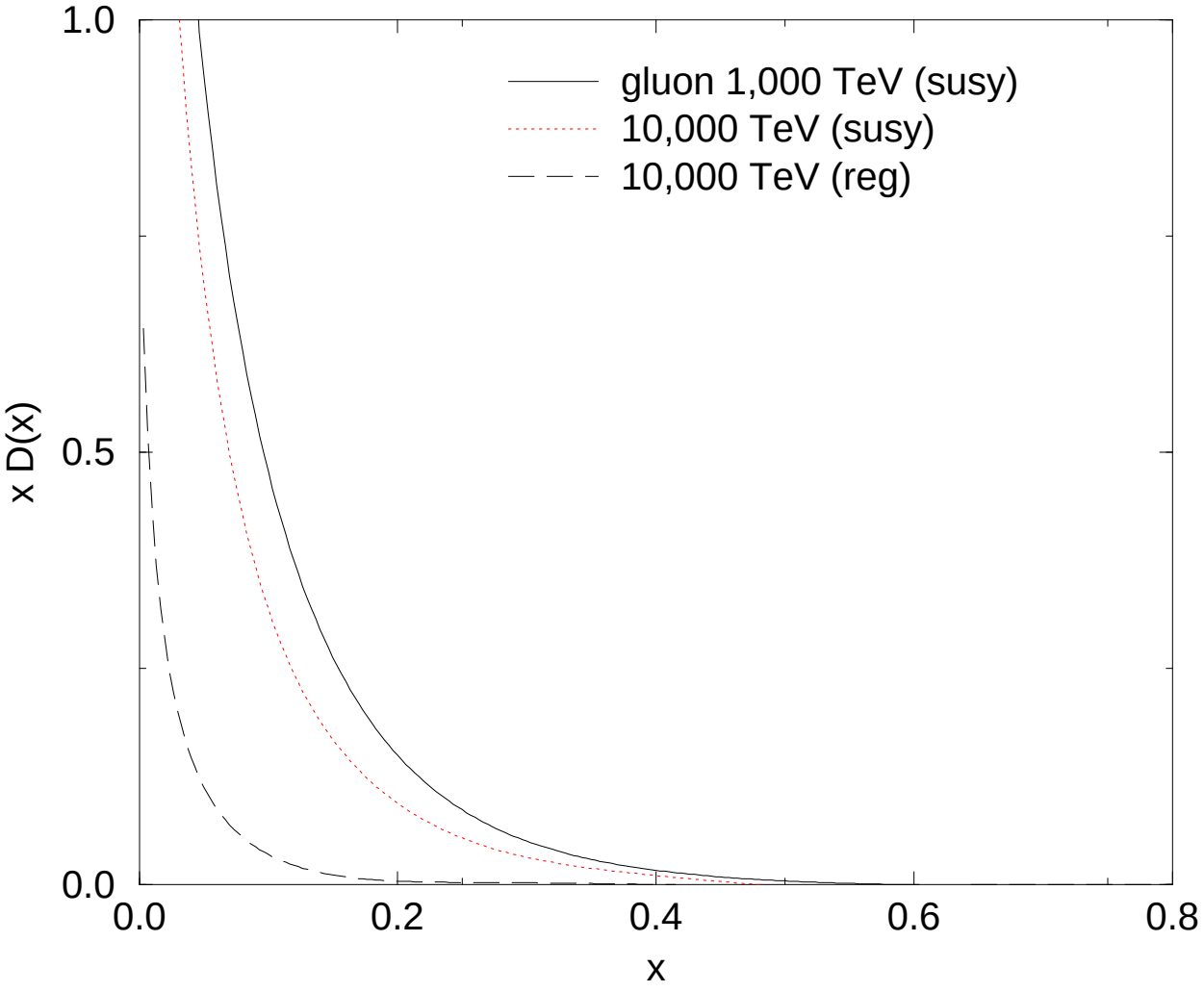
1.0
0.5
0.0
x D(x)
0.0
0.2
0.4
0.6
0.8
x
gluon 1,000 TeV (susy)
10,000 TeV (susy)
10,000 TeV (reg)

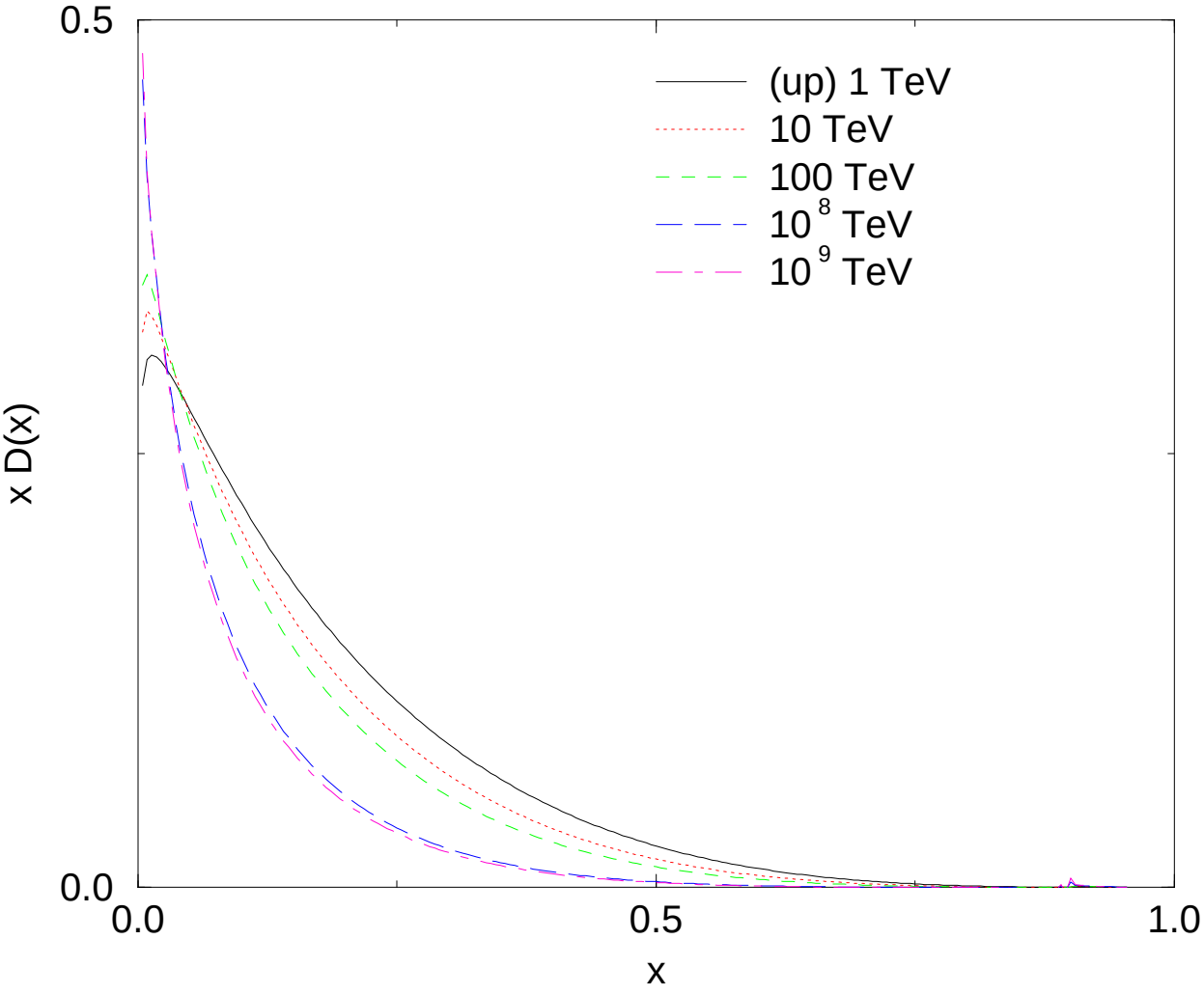
0.5
0.0
0.0
0.5
1.0
x D(x)
x
(up) 1 TeV
10 TeV
100 TeV
10 8 TeV
10 9 TeV